**THE EUROPEAN
PHYSICAL JOURNAL C**

CrossMark

Regular Article - Theoretical Physics

The NMSSM lives: with the 750 GeV diphoton excess

Florian Domingo[1,2], **Sven Heinemeyer**[1,2], **Jong Soo Kim**[1], **Krzysztof Rolbiecki**[1,3,a]

[1] Instituto de Física Teórica (UAM/CSIC), Universidad Autónoma de Madrid, Cantoblanco, 28049 Madrid, Spain
[2] Instituto de Física de Cantabria (CSIC-UC), 39005 Santander, Spain
[3] Institute of Theoretical Physics, University of Warsaw, 02093 Warsaw, Poland

Abstract We propose an NMSSM scenario that can explain the excess in the diphoton spectrum at 750 GeV recently observed by ATLAS and CMS. We show that in a certain limit with a very light pseudoscalar one can reproduce the experimental results without invoking exotic matter. The 750 GeV excess is produced by two resonant heavy Higgs bosons with masses ∼750 GeV, which subsequently decay to two light pseudoscalars. Each of these decays to collimated photon pairs that appear as a single photon in the electromagnetic calorimeter. A mass gap between heavy Higgses mimics a large width of the 750 GeV peak. The production mechanism, containing a strong component via initial b quarks, ameliorates a possible tension with 8 TeV data compared to other production modes. We also discuss other constraints, in particular from low-energy experiments. Finally, we discuss possible methods that could distinguish our proposal from other physics models describing the diphoton excess in the Run-II of the LHC.

1 Introduction

The ATLAS [1] and CMS [2] experiments at the Large Hadron Collider (LHC) have both reported an excess in the diphoton channel at an invariant mass of about 750 GeV corresponding to a local (global) significance of $3.6\,\sigma$ $(2.0\,\sigma)$ and $2.6\,\sigma$ $(1.2\,\sigma)$, respectively. The result is of course not conclusive, but if the excess were confirmed, this would be the first sign of new physics at the terascale energies.

The simplest explanation requires the production of an s-channel spin-0 or spin-2 resonance according to the Yang–Landau theorem [3,4]. The observed cross section of roughly $\mathcal{O}(10)$ fb is relatively large and thus it is natural to assume that the new resonance is produced via the strong interaction and have a large decay rate into diphotons. A light quark initiated resonance would be in severe tension with the LHC Run-I,

since the parton luminosity ratio between $\sqrt{s} = 13$ TeV and 8 TeV is relatively small for light quark initial states. As a consequence, the resonance would have been observed at LHC Run-I if it were produced via quark–antiquark initial states. For a gluon induced resonance the tension with 8 TeV is reduced but still significant [5]. On the contrary, associated production with b quarks does not suffer from 8 TeV constraints. Moreover, the reported event topology is consistent with the single production of a resonance, i.e. non-resonant production of the 750 GeV particle in a cascade decay [6] is disfavored since no additional activity was observed in the peak-region events.[1] Finally, the apparently large width of around 45 GeV, preferred by ATLAS, points to large couplings to its daughter particles. However, strict constraints exist on decays of heavy resonances into electroweak gauge bosons and light Standard Model (SM) fermions and thus the resonance should decay into final states which evade all current experimental searches, implying e.g. a large invisible decay rate or decays to quarks and gluons. Another way out (which we actually consider in this paper) would be the presence of two overlapping resonances with narrow widths which allow one to explain the large width within the current experimental accuracy [8].

The observed diphoton rate cannot be explained with a SM-like Higgs boson because its tree-level decays into third generation quarks and/or gauge bosons are too large compared to the loop induced decays into diphoton final states. However, simple extensions of the SM Higgs sector such as a singlet extension or Two-Higgs-Doublet Model (2HDM) are also plagued with too small diphoton rates and the way out is to introduce new vector-like fermions: see e.g. [9,10]; see [11] for an overview. There are only a few phenomenologically viable explanations within the framework of supersymmetry (SUSY) [12]. It seems to be impossible to find a solu-
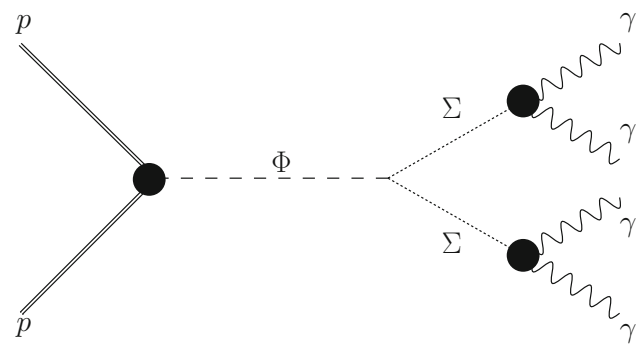
---

[1] However, the heavy parent resonance scenario can still be phenomenologically viable if the lighter resonance mainly decays into dark matter [7].

[a] e-mail: krolb@fuw.edu.pl

Springer

tion within the Minimal Supersymmetric Standard Model (MSSM) [13]. New vector-like fermions and singlets have to be added to the particle spectrum of the MSSM in order to explain the diphoton excess [14–18]. Other SUSY solutions either involves R-parity violation [19,20] or assume a very low SUSY breaking scale [21–23].

The Next-to-Minimal Supersymmetric Standard Model (NMSSM) – see [24,25] for a review – is a well-motivated supersymmetry-inspired extension of the SM. Beyond the elegant features of supersymmetric models in view of the hierarchy problem or one-step unification, and their potential in terms of Dark Matter (DM), the original purpose of the NMSSM rests with the 'μ-problem' [26] of the simpler MSSM: this issue is addressed via the addition of a singlet superfield to the matter content of the MSSM, the 'μ'-parameter then being generated dynamically when the singlet takes a vacuum expectation value (v.e.v.). Additionally, the NMSSM has received renewed attention ever since the Higgs discovery in the Run-I phase of the LHC [27,28], due to its interesting features in terms of a supersymmetric interpretation of the observed Higgs signals – see [29] for a recent analysis and list of references. While several versions of the NMSSM can be formulated, we will focus here on the simplest one, characterized by a Z_3-symmetry and CP-conservation. Let us stress here that we will not include new exotic matter but rely strictly on the simple matter content of this model.

Our purpose in this paper is to present a phenomenologically viable scenario accounting for the diphoton excess at ∼750 GeV in the context of the NMSSM. This explanation rests on the possibility that a $pp \rightarrow \Phi \rightarrow 2(\Sigma \rightarrow \gamma\gamma)$ process – see Fig. 1 – could not be distinguished from a diphoton signal in the experimental searches [30–36]. The NMSSM Higgs sector then offers a suitable framework to embed this topology: Σ can be identified with a very light CP-odd singlet decaying dominantly into a diphoton pair, while heavy CP-even doublet and the CP-even singlet have to be combined to mimic a 750 GeV resonance with adequate properties. Note that contrarily to the proposals which we mentioned earlier, the mechanism that we consider does not rely on the ad hoc inclusion of additional matter (e.g. vector-like fermions) and uses only the existing features and degrees of freedom of a rather simple and well-motivated model.[2] While our project was in its finalizing stages, we became aware of another recent proposal to explain the diphoton signals within the NMSSM [37], which shares some traits with our interpretation but also differs in several respects. The diphoton decay of the pseudoscalar in [37] relies on a substantial 'quasi-mixing' of this Higgs state with the η-meson:

---

[2] We observe also that this mechanism can be transposed to an apparently simpler – in fact theoretically less motivated – singlet extension of the (Type II) 2HDM.

Fig. 1 The resonant production of Φ followed by the decay to two Σ scalars and photons. The final-state photons are pairwise collimated

this requirement induces substantial limits from Υ-decays and results in a quite constrained regime. In our case, we consider the mixing with the π^0 and estimate this effect more quantitatively using the chiral perturbation theory for pions. Moreover, we shall propose a wider selection of benchmark points, illustrating the flexibility of the mechanisms that we employ. Furthermore, we shall analyze in further detail how our scenario compares to the experimental data and study complementary signatures.

In the following section, we will detail how the NMSSM provides an acceptable framework for the ∼750 GeV signal and address several phenomenological issues which constrain the parameter space. We will thus propose specific examples of NMSSM points satisfying these requirements before discussing their relevance in fitting the diphoton excess in Sect. 3. Then we consider other experimental signatures that are specific to our model and have promising prospects in the Run-II, including the decays of the light pseudoscalar to e^+e^- pairs. We also discuss possible experimental signatures from the higgsino, slepton, and heavy Higgs bosons sector. We will conclude with a brief summary in the last section.

2 Embedding the 750 GeV diphoton excess in the parameter space of the NMSSM

The NMSSM Higgs sector – see e.g. [24,25] – consists of two doublets, $H_u = (H_u^+, H_u^0)^T$ and $H_d = (H_d^0, H_d^-)^T$, coupling in a Type II fashion at tree level, as well as a singlet S. Once the Goldstone bosons are rotated away, one is left with a pair of charged states $H^\pm$, two doublet and one singlet CP-even degrees of freedom, h_u, h_d, and h_s, and finally one doublet and one singlet CP-odd components, A_D and A_S. The simplest, Z_3- and CP-conserving version of the NMSSM, which we are considering in this paper, counts seven parameters in the Higgs sector, which can be denoted as $m_{H_u}^2$, $m_{H_d}^2$, m_S^2 – three soft squared masses, λ, κ – two Yukawa-like

supersymmetric couplings, A_λ and A_κ – the two corresponding trilinear soft couplings. It is customary to use the minimization conditions of the Higgs potential to trade three of these parameters, e.g. the soft squared masses, for the Higgs v.e.v.'s, $v_u = \langle H_u^0 \rangle = v \sin\beta$, $v_d = \langle H_d^0 \rangle = v \cos\beta$ (so that $\tan\beta \equiv v_u/v_d$) and $s = \langle S \rangle$. The electroweak properties then imply the identification $v = \left(2\sqrt{2}G_F\right)^{-1/2} \simeq 174$ GeV, G_F representing the Fermi constant. Moreover, in order to provide a more physical handle on the parameter space, we define $\mu \equiv \lambda s$ – which is analogous to its MSSM 'μ' counterpart and also sets the tree-level mass of the higgsino states – and $M_A^2 \equiv \frac{2\lambda s}{\sin 2\beta}(A_\lambda + \kappa s)$ – which sets the scale of an approximate Higgs $SU(2)$-doublet, generally heavy, i.e. $M_A > 125$ GeV, if one wants to avoid the complications of light non-SM-like doublet states.[3] In the following, we shall employ the parameter set $(M_A, \tan\beta, \mu, \lambda, \kappa, A_\kappa)$.

2.1 Identifying the light state 'Σ'

In order to fit the diphoton excess, we want to employ the $pp \to \Phi \to 2(\Sigma \to \gamma\gamma)$ topology. Obviously, Φ would be a CP-even (in order to allow a decay to two lighter identical states) Higgs state at ~ 750 GeV, while Σ could be in principle CP-odd or CP-even: given the limited pool of Higgs states in the NMSSM and the fact that we will have another use for the CP-even singlet (see below), this state will be identified, however, with the singlet-like pseudoscalar. For its diphoton decay to be indistinguishable from a single photon, this Higgs state would have to be light enough: $m_\Sigma \lesssim 0.5$ GeV [32]. We observe that this scenario with a light CP-odd state is phenomenologically viable, in view of the current status of collider constraints. However, severe limits intervene at low mass from, e.g. flavor observables or the properties of the SM-like Higgs boson $H_{\rm SM}$ – a sizable branching fraction $H_{\rm SM} \to \Sigma\Sigma$ would be at odds with the measurements of ATLAS and CMS in the LHC Run-I phase. Note that the Σ state cannot be dominantly doublet in view of the consequences for the spectrum: this would indeed imply the presence of a light charged Higgs (likely in contradiction with limits from top decays [38,39]) and a light CP-even doublet state (in tension with LEP [40,41] and likely to open up sizable unconventional decays of $H_{\rm SM}$).

We complete this discussion with a remark concerning the naturalness of a light CP-odd Higgs in the NMSSM: in two specific limits, this particle appears as the pseudo-Goldstone boson of an approximate symmetry of the Higgs sector:

- for $\kappa \to 0$, i.e. $\kappa \ll \lambda$, the Higgs potential is invariant under a $U(1)$ Peccei–Quinn symmetry, under which

the charges $Q^{\rm PQ}_{H_u, H_d, S}$ of the doublets and singlet satisfy $Q^{\rm PQ}_S + Q^{\rm PQ}_{H_u} + Q^{\rm PQ}_{H_d} = 0$;

- for $A_\kappa, A_\lambda \to 0$, one obtains another $U(1)$ symmetry, with the Higgs charges $Q^R_{H_u, H_d, S}$ satisfying $2Q^R_S - Q^R_{H_u} - Q^R_{H_d} = 0$: this is the R-symmetry limit since the Higgs charges for the specific choice $Q^R_S = -2/3$ coincide with those that these fields would receive under a genuine R-symmetry (also broken by the gaugino masses) of the NMSSM with unbroken supersymmetry. Note that with our choice of parameters, $A_\lambda = -\frac{\kappa}{\lambda}\mu\left(1 - \frac{\lambda M_A^2}{2\kappa\mu^2}\sin 2\beta\right)$ (by definition of M_A).

We will see that, in the scenario under consideration, the factor $\left(1 - \frac{\lambda M_A^2}{2\kappa\mu^2}\sin 2\beta\right)$ has to be small, so that the R-symmetry limit can be invoked.

Most of the characteristics of the NMSSM which intervene in the interpretation of the signal at ~ 750 GeV and the subsequent constraints can be understood from the relations at tree level. This follows from the fact that the relevant physics is driven by comparatively heavy or singlet-like states, for which the radiative corrections are relatively mild in proportion. We shall therefore propose a discussion at tree level in the following. Note, however, that loop corrections play a crucial role for the mass of the SM-like Higgs state so that we will employ tools including leading radiative effects in the numerical analysis (see below). Of course, the exact correlations at tree level are slightly displaced by loop corrections so that small adjustments in the choice of parameters will prove necessary and the relations that we derive below should not be understood as rigid constraints, but rather as qualitative guidelines/trends.

In the base (A_D, A_S), the tree-level squared-mass matrix for the NMSSM CP-odd sector reads

$$\mathcal{M}_P^2 = \begin{bmatrix} M_A^2 & -3\kappa\mu v\left(1 - \frac{\lambda}{6\kappa}\frac{M_A^2}{\mu^2}\sin 2\beta\right) \\ -3\kappa\mu v\left(1 - \frac{\lambda}{6\kappa}\frac{M_A^2}{\mu^2}\sin 2\beta\right) & m_{A_S}^2 \end{bmatrix},$$

$$m_{A_S}^2 \equiv 3\frac{\kappa}{\lambda}\mu\left[-A_\kappa + \frac{\lambda^2 v^2}{2\mu}\sin 2\beta\left(1 + \frac{\lambda}{6\kappa}\frac{M_A^2}{\mu^2}\sin 2\beta\right)\right]. \qquad (1)$$

We observe that the singlet squared-mass $m_{A_S}^2$ is largely determined by the choice of A_κ (since the other terms are small). In particular, low values of A_κ ensure that the singlet is light. Note also that in this case $M_A^2 \gg m_{A_S}^2$ – as we will see later, $M_A \sim 750$ GeV. The subdominant doublet component of the light CP-odd mass state $A_1 = \sqrt{1 - P_d^2}A_S + P_d A_D \simeq A_S + P_d A_D$ can be obtained approximately:

$$P_d \simeq \frac{3\kappa\mu v}{M_A^2}\left(1 - \frac{\lambda}{6\kappa}\frac{M_A^2}{\mu^2}\sin 2\beta\right). \qquad (2)$$

---

[3] A similar quantity would be the mass of the charged-Higgs state: $m_{H^\pm}^2 = M_A^2 + M_W^2 - \lambda^2 v^2$ at tree level. We will prefer M_A in the following since it leads to slightly simpler expressions.

From now on, we identify this light state A_1 to the state Σ of the $pp \to \Phi \to 2(\Sigma \to \gamma\gamma)$ topology.

Now we will address the decays of A_1. For the mass range under consideration, $m_{A_1} \lesssim 0.5$ GeV, the interplay of the pseudoscalar with the strongly interacting sector is non-trivial. In a naive partonic approach, the diphoton decay is significantly suppressed – $\mathcal{O}(10^{-5})$ – for a usual NMSSM pseudoscalar, as long as the competition of the hadronic and muonic final states remains open. Then, below three times the pion mass (the decay to two pions would violate parity), hadronic final states seem inaccessible so that the pseudoscalar would then mainly decay to muons or, below the $\mu^+\mu^-$ threshold, to $\gamma\gamma$ – $\mathcal{O}(70\%)$ at ~ 210 MeV, and the e^+e^- final state would eventually dominate at lower masses ($\lesssim 160$ MeV). Moreover, in such a regime, the pseudoscalar would appear as relatively long lived below the dimuon threshold: the diphoton and e^+e^- final states are essentially mediated by the small doublet component of A_1, resulting in the following (approximate) widths (for $m_{A_1} \lesssim 210$ MeV):

$$\Gamma[A_1 \to e^+e^-] \simeq (1.6 \cdot 10^{-13})\, m_{A_1}\, (P_d \tan\beta)^2,$$
$$\Gamma[A_1 \to \gamma\gamma] \simeq (3 \cdot 10^{-12}\,\text{GeV}^{-2})\, m_{A_1}^3$$
$$\times \left[1 + \left(\frac{m_{A_1}}{0.195\,\text{GeV}}\right)^6\right] (P_d \tan\beta)^2. \tag{3}$$

The corresponding total width is thus of order $\Gamma_{A_1} \sim (10^{-13}\,\text{GeV})\, P_d^2 \tan^2\beta \sim 10^{-14}$ GeV for $P_d \sim 3 \cdot 10^{-2}$, $\tan\beta \sim 10$, and $m_{A_1} \sim 200$ MeV, and narrower at lower masses. The decay length of A_1 at rest is then of order 2 cm. Including the boost factor in the considered topology would lead to a decay length of about 40 m at the LHC, i.e. to an invisible pseudoscalar.

This picture is over-simplistic, however. As [37] already noticed, hadronic effects could substantially affect the decays of A_1. If one were to disregard the tripion threshold for strong-interacting decays, the $s\bar{s}$ and gg final states would completely dominate the partonic decays of A_1, which highlights the sensitivity of the pseudoscalar to the strong sector. In particular, considering the couplings of the pseudoscalar to mesons, one can write the following operators:

$$-\mathcal{L}_{\text{eff}} \ni \delta m_{A_1\pi^0}^2\, A_1\pi^0 + \delta m_{A_1\eta}^2\, A_1\eta + \cdots \tag{4}$$

Such terms induce a mixing of the Higgs pseudoscalars with the pseudoscalar mesons or, in other words, open the possibility for $A_1 \to (\pi^0)^*$ or $A_1 \to (\eta)^*$ decays (the latter being the choice of [37]). The magnitude of the mixing elements $\delta m_{A_1\pi^0/\eta}^2$ can be assessed by rewriting the partonic couplings of A_1 in terms of the axial-flavor currents and their expression in the pion model (chiral perturbation theory) [42–44]:

$$\mathcal{L} \ni -\frac{\iota\, P_d}{\sqrt{2}\,v}$$
$$\times \left\{ m_u \tan^{-1}\beta\, \bar{u}\gamma_5 u + m_d \tan\beta\, \bar{d}\gamma_5 d + m_s \tan\beta\, \bar{s}\gamma_5 s \right\} A_1$$
$$= -\frac{P_d}{2\sqrt{2}\,v}$$
$$\times \partial_\mu \left\{ \tan^{-1}\beta\, \bar{u}\gamma^\mu\gamma_5 u + \tan\beta\, \bar{d}\gamma^\mu\gamma_5 d + \tan\beta\, \bar{s}\gamma^\mu\gamma_5 s \right\} A_1$$
$$= -\frac{P_d}{4v} \left\{ \sqrt{\frac{2}{3}}(\tan^{-1}\beta + 2\tan\beta)\, \partial_\mu J_{A1}^\mu + (\tan^{-1}\beta - \tan\beta)\partial_\mu J_{A3}^\mu \right.$$
$$\left. + \frac{1}{\sqrt{3}}(\tan^{-1}\beta - \tan\beta)\partial_\mu J_{A8}^\mu \right\} A_1$$
$$= -\frac{P_d}{4v} \left\{ \sqrt{\frac{2}{3}}(\tan^{-1}\beta + 2\tan\beta) f_{\eta_1} m_{\eta_1}^2\, \eta_1 + (\tan^{-1}\beta - \tan\beta) f_\pi \right.$$
$$\left. \times \left[m_\pi^2\, \pi_3 + \frac{m_\eta^2}{\sqrt{3}}\, \pi_8 \right] \right\} A_1, \tag{5}$$

where $J_{A1}^\mu = \frac{1}{\sqrt{3}}(\bar{u}\gamma^\mu\gamma_5 u + \bar{d}\gamma^\mu\gamma_5 d + \bar{s}\gamma^\mu\gamma_5 s)$, $J_{A3}^\mu = \frac{1}{\sqrt{2}}(\bar{u}\gamma^\mu\gamma_5 u - \bar{d}\gamma^\mu\gamma_5 d)$, $J_{A8}^\mu = \frac{1}{\sqrt{6}}(\bar{u}\gamma^\mu\gamma_5 u + \bar{d}\gamma^\mu\gamma_5 d - 2\bar{s}\gamma^\mu\gamma_5 s)$ and the divergences of these currents in the pion model are determined by the equations of motion: $\partial_\mu J_{A1}^\mu = f_{\eta_1} m_{\eta_1}^2\, \eta_1$, $\partial_\mu J_{A3}^\mu = f_\pi m_\pi^2\, \pi_3$, and $\partial_\mu J_{A8}^\mu = f_\pi m_\eta^2\, \pi_8$. Here, η_1 denotes the Goldstone field associated with the $U(1)$ axial-flavor symmetry while π_3 and π_8 correspond to the generators $\lambda_3 \equiv \frac{1}{\sqrt{2}}\text{diag}[1, -1, 0]$ and $\lambda_8 \equiv \frac{1}{\sqrt{6}}\text{diag}[1, 1, -2]$ of the $SU(3)$ axial-flavor symmetry. Dismissing the refinements of the π_3, π_8, and η_1 mixings, we can identify $\pi_3 \sim \pi^0$, $\pi_8 \sim \eta$, and $\eta_1 \sim \eta'$. This determines:

$$\delta m_{A_1\pi^0}^2 = \frac{f_\pi}{4v} P_d(\tan^{-1}\beta - \tan\beta)m_\pi^2,$$
$$\delta m_{A_1\eta}^2 = \frac{f_\pi}{4\sqrt{3}\,v} P_d(\tan^{-1}\beta - \tan\beta)m_\eta^2. \tag{6}$$

We observe that these mass-mixing parameters are small: with $f_\pi \simeq 93$ MeV and the typical values $P_d \sim 0.03$ and $\tan\beta \sim 10$, $\delta m_{A_1\pi^0}^2 \sim (4 \cdot 10^{-5} m_\pi^2)$ and $\delta m_{A_1\eta}^2 \sim (2 \cdot 10^{-5} m_\eta^2)$. Therefore, they intervene only in the immediate mass-vicinity of the mesons, and a mixing between A_1 and the mesons of order 10^{-2} thus requires a proximity in mass at the MeV level. In particular, following our analysis, the decay width mediated by a η-state for $m_{A_1} \sim 510$ MeV, as considered in [37], should be completely superseded by e.g. muon decays of A_1. On the other hand, multi-pion decays are still kinematically open for $m_{A_1} \sim 510$ MeV, which may result in multi-photon final-states. We shall not elaborate further on this possibility and we now focus on the mixing of A_1 with π^0, i.e. assume $m_{A_1} \sim 135$ MeV. At first order in $\delta m_{A_1\pi^0}^2$, the mixing angle θ reads $\theta \simeq \delta m_{A_1\pi^0}^2/(m_\pi^2 - m_{A_1}^2)$ and the mass shift driven by mixing is $\frac{m_\pi \theta^2}{2}\left|1 - \frac{m_{A_1}^2}{m_\pi^2}\right|$: for a mixing of order $\theta \sim 10^{-2}$ it translates into a (completely negligible) sub-keV correction. A sample plot of the mixing angle as a function of the A_1 mass for fixed P_d is shown in the left
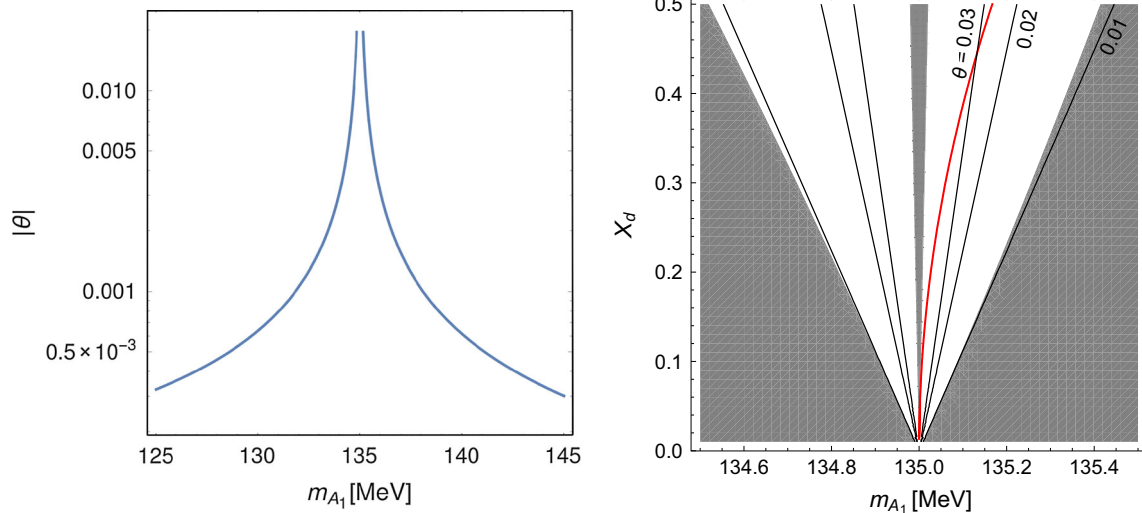
Fig. 2 *Left* the mixing angle $|\theta|$ as a function of A_1 mass for $P_d = 0.035$ and $\tan\beta = 10$. *Right* the contours (*black*) of the mixing angle $\theta = 0.01, 0.02, 0.03$ (from the most outer) in the m_{A_1}–X_d plane where $X_d = P_d(\tan\beta - 1/\tan\beta)$ and $\tan\beta = 10$. The *gray*-shaded regions are excluded; see the *text* for details. The *red* contour denotes the value of mixing required to recover the experimental central value for BR$[\pi^0 \to e^+e^-]$ (hence resolve the discrepancy)

panel of Fig. 2. As an example, for $P_d = 0.035$, $\tan\beta \simeq 10$, and $|m_{A_1} - m_\pi| < 0.3$ MeV we find $\theta = 10^{-2}$. The consequences for the decays of A_1 are sizable: via its small π^0 component, the pseudoscalar acquires pion-like decays with values about

$$\Gamma_{A_1}^\pi \simeq \theta^2\,\Gamma_\pi \sim 8 \cdot 10^{-13}\ \text{GeV}, \tag{7}$$

essentially to $\gamma\gamma$ (BR$[\pi^0 \to \gamma\gamma] \sim 99\,\%$), which overrule the 'pure-Higgs' decays of order 10^{-15} GeV. The decay length in the lab frame for the process of Fig. 1 is then reduced to ~ 0.5 m, placing most of the time the decay vertex to photons before A_1 reaches electromagnetic calorimeter.[4] Even shorter decay lengths are possible for larger A_1–π^0 mixing. For the pion, on the other hand, the consequences are minimal as its natural decays are slightly decreased at the level of 0.01 % (far below the theoretical or experimental precisions) and slightly shifted by a Higgs-like width at the level of 10^{-16}–10^{-17} GeV (via interference terms). The 2σ experimental error on the pion decay width to two photons of 4 % defines our upper limit on the mixing.[5] In the right

panel of Fig. 2 we show contours of the constant mixing angle θ in the m_{A_1}–X_d plane. With the above constraints, the regions shaded in gray are excluded. The central part around $m_{A_1} \simeq 135$ MeV is excluded by the upper limit of the measurement of the width $\Gamma[\pi^0 \to \gamma\gamma]$, while the outer part by A_1 decay length at the LHC, which would be larger than ~ 0.5 m. It should be noted that the Particle Data Group [47] reports BR$[\pi^0 \to e^+e^-] = (6.46 \pm 0.33) \cdot 10^{-8}$ leading to a width $\Gamma[\pi^0 \to e^+e^-] \simeq 5 \cdot 10^{-16}$ GeV, known at the 6 % level. Inclusion of radiative corrections shifts this value to BR$[\pi^0 \to e^+e^-] = (7.48 \pm 0.38) \cdot 10^{-8}$ [48], while the recent theoretical calculation gives $(6.2 \pm 0.1) \cdot 10^{-8}$ [49], so that the inclusion of new physics at this level may even be welcome: see e.g. [50]. In our case, the red contour in Fig. 2 denotes the mixing angles that could account for the discrepancy in $\pi^0 \to e^+e^-$ (considering the central values only).

In the following, we will assume that this mixing mechanism between A_1 and π^0 is responsible for the apparent A_1 width— resulting in a decay length of order $\lesssim 0.5$ m for the topology of Fig. 1 – and a BR$[A_1 \to \gamma\gamma] \simeq 99\,\%$.

2.2 Identifying the heavy state 'Φ'

We now turn to the CP-even sector. In the base ($H_{SM} = \cos\beta\,h_d + \sin\beta\,h_u$, $H_D = -\sin\beta\,h_d + \cos\beta\,h_u$, $H_S = h_s$), the tree-level squared-mass matrix reads

---

[4] We observe that for such decay lengths, the configuration of ATLAS with a ECAL detector farther from the beam could make this experiment more sensitive to the process than the more compact CMS, which could lead to a slightly weaker signal in CMS (roughly in agreement with the current experimental situation).

[5] It should be noted that the measured value of $\Gamma[\pi^0 \to \gamma\gamma]$ is slightly below the most recent theoretical calculations; see [45]. We note that the mixing discussed here could help to explain this tension. We speculate that the experimental setup similar to the one used for a direct measurement of the pion decay length [46], could also detect A_1 once the detectors are moved farther away from the target. By observing

Footnote 5 continued
a change in the measured mean decay length one could directly probe parameters of A_1–π^0 mixing.

$$
\mathcal{M}_S^2 = \begin{bmatrix} M_Z^2 \cos^2 2\beta + \lambda^2 v^2 \sin^2 2\beta & (\lambda^2 v^2 - M_Z^2)\sin 2\beta \cos 2\beta & 2\lambda\mu v\left[1 - \left(\frac{M_A \sin 2\beta}{2\mu}\right)^2\right] \\ (\lambda^2 v^2 - M_Z^2)\sin 2\beta \cos 2\beta & M_A^2 + (M_Z^2 - \lambda^2 v^2)\sin^2 2\beta & -\frac{\lambda v}{2\mu} M_A^2 \sin 2\beta \cos 2\beta \\ 2\lambda\mu v\left[1 - \left(\frac{M_A \sin 2\beta}{2\mu}\right)^2\right] & -\frac{\lambda v}{2\mu} M_A^2 \sin 2\beta \cos 2\beta & m_{H_S}^2 \end{bmatrix},
$$

$$
m_{H_S}^2 \equiv \left(\frac{2\kappa}{\lambda}\mu\right)^2\left[1 + \frac{\lambda A_\kappa}{4\kappa\mu}\right] - \frac{\kappa\lambda}{2}v^2 \sin 2\beta\left[1 - \frac{\lambda M_A^2}{\kappa\mu^2}\right]. \tag{8}
$$

It should be noted that, as long as $M_A \gg v$, the doublet sector is approximately diagonal and that the mass of the heavy doublet state H_D falls close to M_A. Moreover, keeping in mind that A_κ is small in order to ensure a light A_1, we observe that the mass of the CP-even singlet H_S is dominated by the term $\frac{2\kappa}{\lambda}\mu$, as long as this quantity is larger than $\mathcal{O}(v)$. In such a regime, the lightest CP-even Higgs state H_1 can thus be identified with H_{SM} (approximately): $H_1 \simeq \sqrt{1 - S_{13}^2}\, H_{SM} + S_{13}\, H_S$, where the singlet component is very small: $S_{13} \ll 1$. Consequently, the H_1 behaves SM-like, in agreement with the experimental results [51].

We now want to identify the state Φ of the $pp \to \Phi \to 2(\Sigma \to \gamma\gamma)$ topology with one of the CP-even states of the NMSSM. The associated mass should fall close to ~ 750 GeV. Both H_D and H_S are potential candidates. However, the Φ state should be sizably produced at the LHC, which implies a significant coupling to SM particles, such as gluons or quarks. In the case of a dominantly singlet state, such couplings are typically suppressed in proportion to the small doublet component of the state. On the other hand, H_D has sizable couplings to tops (though $\tan^{-1}\beta$ suppressed with respect to the SM) and to bottom quarks ($\tan\beta$-enhanced), so that a measurable production in gluon–gluon fusion (ggf) or in association with b's (bbh) is plausible. We observe that the production cross section of a 750 GeV H_D in ggf at 13 TeV is well approximated by $(0.6\text{ pb})/\tan^2\beta$ for $\tan\beta \lesssim 15$, and the bbh cross section, by $(4\cdot 10^{-4}\text{ pb}) \times \tan^2\beta$. The production cross section would thus point toward an identification $\Phi \sim H_D$, which would imply $M_A \sim 750$ GeV.

Yet, another consideration is that Φ should have a large decay into a pair of A_1's. Naively, the SM fermionic final states would offer a sizable competition:

$$
\Gamma[\Phi \to t\bar{t}] \sim \frac{3 G_F m_t^2}{4\sqrt{2}\pi} m_\Phi
$$
$$
\times \left(1 - 4\frac{m_t^2}{m_\Phi^2}\right)^{3/2}\left(\frac{g_{\Phi t\bar{t}}}{g_{\Phi t\bar{t}}^{SM}}\right)^2 \sim (30\text{ GeV})\left(\frac{g_{\Phi t\bar{t}}}{g_{\Phi t\bar{t}}^{SM}}\right)^2, \tag{9}
$$

$$
\Gamma[\Phi \to b\bar{b}] \sim \frac{3 G_F m_b^2}{4\sqrt{2}\pi} m_\Phi \left(1 - 4\frac{m_b^2}{m_\Phi^2}\right)^{3/2} \tag{10}
$$

$$
\times \left(\frac{g_{\Phi b\bar{b}}}{g_{\Phi b\bar{b}}^{SM}}\right)^2 \sim (0.03\text{ GeV})\left(\frac{g_{\Phi b\bar{b}}}{g_{\Phi b\bar{b}}^{SM}}\right)^2,
$$

with $m_\Phi \simeq 750$ GeV and the relative fermionic couplings to their SM counterparts $\frac{g_{\Phi t\bar{t}}}{g_{\Phi t\bar{t}}^{SM}}$ and $\frac{g_{\Phi b\bar{b}}}{g_{\Phi b\bar{b}}^{SM}}$. On the other hand, the decay width into $2A_1$ can be estimated as (still for $m_\Phi \sim 750$ GeV):

$$
\Gamma[\Phi \to A_1 A_1] = \frac{g_{\Phi A_1 A_1}^2}{32\pi m_\Phi}\sqrt{1 - 4\frac{m_{A_1}^2}{m_\Phi^2}}
$$
$$
\simeq (1\cdot 10^{-5}\text{ GeV}^{-1})\, g_{\Phi A_1 A_1}^2. \tag{11}
$$

For the heavy doublet state, the fermionic couplings are approximately determined by $\tan\beta$: $\frac{g_{H_D t\bar{t}}}{g_{H_D t\bar{t}}^{SM}} \simeq \tan^{-1}\beta$ and $\frac{g_{H_D b\bar{b}}}{g_{H_D b\bar{b}}^{SM}} \simeq \tan\beta$. The fermionic channels will thus typically give a width of order 1 GeV at least, for moderate $\tan\beta = \mathcal{O}(10)$. On the other hand, the leading terms in the couplings of a CP-even doublet with a pair of CP-odd singlets read $g_{H_D A_1 A_1} \sim \sqrt{2}\lambda(\lambda + \kappa)\cos 2\beta\, v$. Considering $\lambda, \kappa = \mathcal{O}(0.1)$ – in any case, $\lambda^2 + \kappa^2 \lesssim 0.5$ if we want the model to remain perturbative up to the GUT scale, we observe that $\Gamma[H_D \to A_1 A_1] \ll \mathcal{O}(\text{GeV})$, so that the associated branching ratio is suppressed in view of the fermionic channels. On the other hand, for H_S, the decay channels into SM particles are naturally suppressed while the decay into light CP-odd singlets is large: $\Gamma[H_S \to A_1 A_1]$ can be read from Eq. (11) with the replacement $g_{\Phi A_1 A_1} \leftarrow g_{H_S A_1 A_1} \sim \sqrt{2}\kappa\left(2\frac{\kappa}{\lambda}\mu - A_\kappa\right)$. If this state H_S were at ~ 750 GeV, then $2\frac{\kappa}{\lambda}\mu \simeq 750$ GeV, while A_κ is negligible (from the low mass of the CP-odd singlet). We thus obtain that $\Gamma[H_S \to A_1 A_1]$ is of order 1 GeV, as long as $\kappa \gtrsim 0.25$. Therefore, the branching ratio[6] $\Phi \to \Sigma\Sigma$ pleads for the identification $\Phi \sim H_S$, hence $2\frac{\kappa}{\lambda}\mu \simeq 750$ GeV. These two apparently conflicting requirements, $\Phi \sim H_D$ for the production and $\Phi \sim H_S$ for the decay, can actually be reconciled if one keeps in mind that the mass states H_2 and H_3 are in fact admixtures (essentially)

---

[6] It should be noted that the other singlet-like channel $H_S \to \tilde{\chi}_s\tilde{\chi}_s$, $\tilde{\chi}_s$ denoting the singlino state, is kinematically closed, as the singlino mass is also of order $2\frac{\kappa}{\lambda}\mu \simeq 750$ GeV.

of H_D and H_S. Provided the mixing is large, then the mass states will combine the properties of both their doublet and singlet CP-even components. Two interpretations are then possible for Φ:

- The first is that the diphoton excess corresponds to only one of the two states H_2 or H_3, while the other would give a subdominant effect due to the details of the singlet–doublet mixing. Considering the somewhat large width of order $\mathcal{O}(45 \text{ GeV})$ which seems associated with the excess, this interpretation tends to imply a very large $\Gamma[H_S \to A_1 A_1] = \mathcal{O}(45 \text{ GeV})$, which could only be achieved with $\kappa \geq 1$, that is, outside the perturbative regime. We will not discuss this scenario any further.[7]

- The second possibility is that both states are sufficiently close in mass to appear as a single excess. The very large binning makes such a scenario plausible, even for mass differences of order $\mathcal{O}(20–40 \text{ GeV})$. Then, whatever the width of the physical states H_2 and H_3, the associated signal would like a broad resonance; this will be discussed in Sect. 3.1. From previous considerations, we see that the actual widths of H_2 and H_3 in the considered regime would be of order $\mathcal{O}(1 \text{ GeV})$. Their minimal mass difference (for a maximal mixing) can be inferred from the off-diagonal element of the squared-mass matrix Eq. (8):

$$m_{H_3} - m_{H_2}\big|_{\min} \simeq \frac{\kappa v}{2} |\sin 4\beta|, \tag{12}$$

where we have used $M_A \simeq 750 \text{ GeV} \simeq 2\frac{\kappa}{\lambda}\mu$. For $\kappa = \mathcal{O}(0.3)$ and $\tan \beta = \mathcal{O}(10)$, we obtain a typical spread of 10 GeV in mass. This is the scenario we will be focusing on in the following.

From now on, we thus assume $M_A \simeq 750 \text{ GeV} \simeq 2\frac{\kappa}{\lambda}\mu$, which causes a strong mixing between H_D and H_S, so that $H_{2,3} \sim \frac{1}{\sqrt{2}}[H_D \pm H_S]$, both states having masses close to 750 GeV.

[7] While our study was already in progress, we became aware of the discussion in [52].

2.3 Other phenomenological constraints

After identifying how the NMSSM Higgs spectrum could provide an interpretation of the diphoton excess via the $pp \to \Phi \to 2(\Sigma \to \gamma\gamma)$ topology, we will consider additional constraints and consequences on this scenario.

The SM-like properties of the Higgs state at $\sim 125 \text{ GeV}$ place a major phenomenological limit on the existence of a light pseudoscalar: as a general rule, the channel $H_{\text{SM}} \to A_1 A_1$ should remain subdominant – compared to the SM width $\Gamma_{\text{SM}} \simeq 4 \text{ MeV}$ – or it would induce a sizable unconventional decay of the state at $\sim 125 \text{ GeV}$, which would cause tensions with the results of the LHC Run-I. In our case, with a very light A_1 being experimentally indistinguishable from a photon, the limits on $H_{\text{SM}} \to A_1 A_1$ are even more severe in order to avoid a large apparent decay $H_{\text{SM}} \to \gamma\gamma$, again in contradiction with the Run-I results. The corresponding width can be estimated as

$$\Gamma[H_{\text{SM}} \to A_1 A_1] = \frac{g^2_{H_{\text{SM}}A_1A_1}}{32\pi m_{H_{\text{SM}}}}$$

$$\times \sqrt{1 - 4\frac{m^2_{A_1}}{m^2_{H_{\text{SM}}}}} \simeq (8 \cdot 10^{-5} \text{ GeV}^{-1}) g^2_{H_{\text{SM}}A_1A_1}. \tag{13}$$

The condition $\Gamma[H_{\text{SM}} \to A_1 A_1] \ll \Gamma_{\text{SM}} \cdot \text{BR}^{\text{SM}}[H_{\text{SM}} \to \gamma\gamma] \sim 8 \cdot 10^{-6} \text{ GeV}$ translates into $g_{H_{\text{SM}}A_1A_1} < 0.3 \text{ GeV}$. The tree-level coupling $g_{H_{\text{SM}}A_1A_1}$ reads

$$\frac{g_{H_{\text{SM}}A_1A_1}}{\sqrt{2}} \simeq -\kappa A_\kappa S_{13}(1 - P_d^2) + \left[\lambda^2 \cos^2 \beta - \frac{1}{2}\left(\frac{M_Z}{v}\right)^2 \cos^2 2\beta\right] v \sqrt{1 - S_{13}^2} P_d^2$$

$$+ \lambda \mu \left[1 + \frac{\kappa}{2\lambda} \sin 2\beta \left(1 + \frac{\lambda}{2\kappa} \frac{M_A^2}{\mu^2} \sin 2\beta\right)\right] S_{13} P_d^2 - 2\lambda \kappa v S_{13} P_d \sqrt{1 - P_d^2}$$

$$+ \lambda (\lambda + \kappa \sin 2\beta) v \sqrt{1 - S_{13}^2}(1 - P_d^2) - 3\kappa\mu \left[1 - \frac{\lambda}{6\kappa}\frac{M_A^2}{\mu^2}\sin 2\beta\right] \sqrt{1 - S_{13}^2}\sqrt{1 - P_d^2} P_d. \tag{14}$$

One should observe that, typically, $\lambda, \kappa = \mathcal{O}(0.1)$, $2 < \tan \beta \lesssim \mathcal{O}(10–20)$, and $S_{13}, P_d \ll 1$. As a result, the two 'dangerous' terms in Eq. (14) are those of the last line. Considering Eq. (2) and $S_{13}, P_d \ll 1$, the condition on $g_{H_{\text{SM}}A_1A_1}$ implies

$$\lambda^2 v \left|1 + \frac{\kappa}{\lambda}\sin 2\beta - \frac{9}{4}\left(\frac{2\kappa\mu}{\lambda M_A}\right)^2\left[1 - \frac{\lambda}{6\kappa}\frac{M_A^2}{\mu^2}\sin 2\beta\right]\right|$$

$$< 0.2 \text{ GeV} \Rightarrow \lambda^2\left[1 - \frac{2\kappa}{\lambda}\sin 2\beta\right] \lesssim 1 \cdot 10^{-3}, \tag{15}$$

where we have applied the mass condition $M_A \simeq 750 \text{ GeV} \simeq 2\frac{\kappa}{\lambda}\mu$ for the final step.

A first alternative would thus consist in choosing $\lambda \lesssim 3 \cdot 10^{-2}$, which will also lead to $\kappa \lesssim 0.1$: then, however, the

decay $H_S \rightarrow A_1 A_1$ no longer competes with the fermionic decays of H_D and the mixing among H_S and H_D is reduced. Our scenario would thus be invalidated. We will thus prefer to keep $\lambda \gtrsim 0.1$ and satisfy the limit from $\Gamma[H_{SM} \rightarrow A_1 A_1]$ with the condition $\frac{\kappa}{\lambda} \sin 2\beta \sim 0.5$. It should be noted that this condition is actually less ad hoc than it looks at first glance: indeed, given the mass condition $M_A \simeq 750$ GeV $\simeq 2\frac{\kappa}{\lambda}\mu$, $A_\lambda \simeq -\frac{M_A}{2}\left[1 - \frac{2\kappa}{\lambda}\sin 2\beta\right]$, so that, together with the requirement of a small A_κ, the assumption $\frac{\kappa}{\lambda} \sin 2\beta \sim 0.5$ places us naturally in the R-symmetry limit of the NMSSM.

On the other hand, the perturbativity of the couplings up to the GUT scale approximately implies $\lambda^2 + \kappa^2 \lesssim 0.5$. Using the condition $\frac{\kappa}{\lambda} \sin 2\beta \sim 0.5$ then places an upper bound on $\lambda \lesssim \sin 2\beta \sqrt{\frac{2}{1+4\sin^2 2\beta}}$. Moreover, our scenario requires that the width $\Gamma[H_S \rightarrow A_1 A_1]$ remains competitive in view of the fermionic decays of H_D, $\Gamma[H_D \rightarrow t\bar{t}/b\bar{b}]$: considering the production cross sections of H_D, the efficient branching ratio $BR[A_1 \rightarrow \gamma\gamma] \simeq 0.99$, mediated by the pion, and the magnitude of the diphoton excess at ATLAS and CMS, the condition on κ can be lowered to $\kappa \gtrsim 0.1$ – instead of 0.25 as we discussed above – and translates into a lower bound of $\lambda \sim 2\kappa \sin 2\beta \gtrsim 0.2 \sin 2\beta$.

A further implication of $\frac{\kappa}{\lambda} \sin 2\beta \sim 0.5$ together with the mass condition $M_A \simeq 750$ GeV $\simeq 2\frac{\kappa}{\lambda}\mu$ reads $\mu \sim M_A \sin 2\beta$. An immediate consequence is that $\mu \leq 750$ GeV, and even $\mu \leq 375$ GeV as soon as $\tan\beta \gtrsim 3.7$, so that the higgsino states will typically be light, i.e. for $\tan\beta \gtrsim 3.7$ H_2 and H_3 can have a non-negligible decay rate to higgsinos. This will dilute somewhat more the $H_{2,3} \rightarrow A_1 A_1$ rates, although the typical widths are of order $\sim(15 \text{ GeV})\lambda^2\left(1 - \frac{\lambda^2}{\kappa^2}\right)^{3/2}$. While nothing forbids that the gauginos also intervene at a low mass, we will assume in the following that they are heavier. A neutral higgsino is thus the lightest supersymmetric particle (LSP), which is consistent with cosmological limits on the dark matter density: the thermal higgsino relics are typically below the observed value of the relic density [12]. However, scenarios with low thermal relic density can be consistent with the measured abundance [53–55].

However, μ cannot be too small, since this would contradict the unsuccessful results of LEP in chargino searches [56]. Using the limit $\mu \gtrsim 100$ GeV then provides a bound on $\tan\beta$, in which the choice $\frac{\kappa}{\lambda} \sin 2\beta \sim 0.5$ can be conciliated with the mass requirement $M_A \simeq 750$ GeV $\simeq 2\frac{\kappa}{\lambda}\mu$: $\tan\beta \lesssim 15$.

In [37], limits from Υ decays play a determining role in constraining the parameter space: the Wilson formula [57] gives $BR[\Upsilon(1S) \rightarrow \gamma A_1] \sim 1 \cdot 10^{-4}$ $(P_d \tan\beta)^2$, which would typically lead to a $\sim 10^{-6}$–10^{-5} effect in $\Upsilon(1S)$ radiative decays (and similar values for $\Upsilon(2, 3S)$). However, we are not aware of experimental limits applying to a pseudoscalar with mass close to that of the pion. Searches in radiative Υ decays typically ignore mass scales below

0.2 GeV, except for invisible final states, which are not relevant in our scenario. Similar contributions of the A_1 to the radiative decays of J/ψ are suppressed, due to the smaller charm mass and the $\tan^{-2}\beta$ suppression of the A_1-charm coupling. Furthermore, as in [37], we find that the impact of A_1 in radiative Z-decays is orders of magnitude below the experimental bounds [47,58].

As [59] pointed out, the presence of a light Higgs pseudoscalar generically leads to tensions in flavor physics. Limits from invisible decays do not apply in our scenario, as A_1 would decay within ~ 1 cm at B-factories, but the rare transitions $B \rightarrow K e^+ e^-$ and $K \rightarrow \pi e^+ e^-$ should be considered carefully. Indeed, following [60], one observes that such transitions can be mediated by a light A_1, as $BR[A_1 \rightarrow e^+ e^-]$ is sizable (at the percent level) below the $\mu^+\mu^-$ threshold. The strongest limit comes from [61]:

$$BR^{NA48/2}(K^\pm \rightarrow \pi^\pm e^+ e^-) = (3.11 \pm 0.12) \times 10^{-7}. \quad (16)$$

The actual bound is in fact much stronger than one can infer from the decay rate alone. The $e^+ e^-$ spectrum is well measured [61], with low background and small theory uncertainty: therefore a peak in the $e^+ e^-$ invariant mass spectrum would be clearly visible. This implies that the A_1 contribution has to be strongly suppressed: even though, in our configuration, $BR[A_1 \rightarrow e^+ e^-]$ falls below the percent level due to the large pion-mediated width, the typical magnitude of the effective $\bar{b}sA_1$ and $\bar{s}dA_1$ couplings, $C_A \sim 10^2$–10^3 GeV^2 and $C_A' \sim 10^0$–10^1 GeV^2, would result in an excess – see e.g. Eqs. (21) and (25) in [59]. The conclusion that these flavor-changing processes exclude the considered scenario would be premature, however. First, one should keep in mind that such A_1-mediated signals may hide in the background of the pion, due to the proximity in mass. Then the actual size of C_A and C_A' depends on the details of the sfermion spectrum and, in particular, these coefficients vanish in the super-GIM limit [60]. The sfermion sector is largely free in what precedes our analysis: its only role so far was to ensure the correct mass for the SM-like state via radiative corrections – this essentially translates into a scalar top spectrum of a few TeV, or very large mixing in the stop sector. We check that C_A and C_A' can be made arbitrarily small for suitable choices of the squark spectra, so that flavor constraints – and not only those involving a $A_1 \rightarrow e^+ e^-$ decay – can be generally circumvented; see benchmark point P2 below.

More general limits on the spectra, such as $B \rightarrow X_s \gamma$ or $B_s \rightarrow \mu^+\mu^-$, should also be considered [62], but note that the already large $m_{H^\pm} \simeq 750$ GeV, the moderate value of $\tan\beta$, the flexibility of the squark spectra, and the fact that A_1 is off-resonance contrive to place our scenario within 95 % of these flavor constraints.

In Ref. [59] it was argued that important constraints on Higgs-like pseudoscalars can be obtained in beam dump

experiments. The most sensitive one is the CHARM search for axions [63]. Using Eq. (3) of Ref. [63] one can estimate the F_X parameter to be $F_X < 10$ GeV, assuming that $\Gamma[A_1 \to \gamma\gamma]/\Gamma[\pi^0 \to \gamma\gamma] > 10^{-4}$ as required by the decay length $\lesssim 0.5$ m of A_1 at the LHC. Looking at the exclusion plot in Fig. 4 of [63] one immediately sees that this is way below sensitivity of the experiment. In any case, with this decay length at the LHC, the decay length at CHARM would be of order $\mathcal{O}(1)$ cm. After 60 cm the flux suppression would be $\sim 2^{60} \simeq 10^{18}$. Taking into account that the CHARM detector was 480 m away from the target and that initial A_1 flux was $< 10^{17}$ one clearly sees that possibly no pseudoscalars could have reached the detector.

Finally, the anomalous magnetic moment of the muon may also be of relevance: a light A_1 is indeed known to widen the discrepancy between the prediction of the model and the experimental measurement; see [64]. Yet, the moderate value of $\tan \beta$ and the presence of light higgsinos concur to make the supersymmetric corrections to $(g - 2)_\mu$ the dominant new-physics effect. The overall contribution thus improves the agreement with the BNL measurement as compared to the SM. Placing $(g - 2)_\mu$ within 2σ of the experiment remains problematic, however, and can be achieved only in the upper reach of $\tan \beta \sim 15$. It should be noted that this observable depends on the details of the slepton masses, such that lighter smuons and sneutrinos would improve the situation. The LHC searches on light neutralinos and sleptons will be discussed in the following section.

2.4 Favored parameter space

To summarize this analysis, it appears that most of the parameters in the NMSSM Higgs sector are fixed or bounded in the scenario that we consider:

- $M_A \simeq 750$ GeV enables a sizable production of the state(s) at ~ 750 GeV via a significant H_D component;
- $\kappa \simeq \frac{\lambda}{2\sin 2\beta}$ ensures a suppressed decay $H_{\mathrm{SM}} \to A_1 A_1$; furthermore, $\kappa \gtrsim 0.1$ allows for a competitive $\Gamma[H_S \to A_1 A_1]$ as compared to the fermionic decays of H_D; finally, κ determines the separation in mass for the states at ~ 750 GeV;
- $\mu \sim M_A \sin 2\beta$ is fixed both by the requirement $2\frac{\kappa}{\lambda}\mu \simeq 750$ GeV, conditioning the presence of a singlet-like component at ~ 750 GeV, with the significant decay to pseudoscalars, and by the condition on $H_{\mathrm{SM}} \to A_1 A_1$;
- λ is bounded as $\frac{0.4\tan\beta}{1+\tan^2\beta} \lesssim \lambda \lesssim \frac{2\sqrt{2}\tan\beta}{\sqrt{1+18\tan^2\beta+\tan^4\beta}}$: this results from the conditions of a suppressed decay $H_{\mathrm{SM}} \to A_1 A_1$, which would spoil the interpretation of the LHC Run-I results, of perturbativity up to the GUT scale and of a sizable $\Gamma[H_S \to A_1 A_1]$; moreover, the light CP-odd Higgs would be long lived if λ were too small;

- $\tan \beta \lesssim 15$ is constrained by the lower bound on chargino searches $\mu \gtrsim 100$ GeV, as a result of the various correlations; note that $\tan \beta = \mathcal{O}(10)$ satisfies the requirements on the fermionic decays of the states at ~ 750 GeV – which should remain moderate;
- $A_\kappa \lesssim \mathcal{O}(0.1)$ GeV conditions a light CP-odd singlet; note that, together with the requirement $A_\lambda \to 0$, which, in our scenario, follows the assumptions on κ, λ, μ, and $M_A, A_\kappa \to 0$ places us in the approximate R-symmetry limit of the NMSSM, and that A_1 thus appears as the pseudo-Goldstone boson of this R-symmetry.

Moreover, the requirements of a ~ 125 GeV mass for the SM-like Higgs state and flavor physics constrain the squark spectra, while $(g - 2)_\mu$ and slepton searches impact the slepton spectrum. We stress that the singlino and higgsino masses are essentially determined by the choices in the Higgs sector and that light higgsinos (constituting the LSP in the simplest configuration) appear as a trademark of this scenario.

It should be noted that most of the properties of the Higgs sector can be transposed to a simpler singlet extension of the 2HDM, without the complications in the supersymmetric spectrum and with increased number of parameters and degrees of freedom. In the latter setup, one should consider the low-energy constraints more carefully, however, as charged-Higgs contributions to $B \to X_s \gamma$ can no longer be balanced by the SUSY loops and the anomalous magnetic moment of the muon would suffer from the negative contributions driven by the loop involving the muon and the light pseudoscalar if the 2HDM is of Type II (which determines the production of the states at ~ 750 GeV). It should be kept in mind that the singlet + 2HDM framework receives no deep motivation from the hierarchy problem, DM or gauge unification.

Naturally, certain attractive features of the NMSSM Higgs sector, such as the possibility of a light CP-even singlet, appear as a necessary sacrifice in order to conciliate an interpretation of the ~ 750 GeV excess with the parameter space and constraints of the NMSSM. Moreover, it could be argued that the mechanisms which we invoke – from the sizable singlet–doublet mixing at ~ 750 GeV, or the condition of a A_1–π^0 interplay, to the collimated diphoton decays, indistinguishable from a single photon – are quite elaborate. Still, it is remarkable that all the necessary properties to fit the signal can be united in a phenomenologically realistic way within as theoretically simple a model as the NMSSM, without e.g. requiring additional ad hoc matter.

2.5 Benchmark points

To investigate the NMSSM parameter space more thoroughly than the derivation at tree level allows, and account for e.g.

higher-order corrections or verify various phenomenological constraints, we use the public package `NMSSMTools` `4.8.2` [65–67]. The Higgs spectrum is computed with precision setting 2, i.e. including full one-loop, Yukawa-driven two-loop as well as pole corrections [68]. Note that we dismiss the width and branching fractions computed by this code for the light A_1 as they do not implement the effect of hadronic states. We simply tune the mass m_{A_1} to ~ 135 MeV and then invoke a mixing with the pion at the level of $\theta \sim 10^{-2}$ – in practice, this might require further adjustment in the choice of m_{A_1} but this can be achieved with completely negligible consequences for the rest of the spectrum. Additionally, `NMSSMTools` is interfaced [29] with `HiggsBounds` `4.2.1` [69–72] and `HiggsSignals` `1.4.0` [73] in order to test the properties of the Higgs sector in view of current collider limits. However, we still have to check 'by hand' that the decay $H_1 \rightarrow A_1 A_1$ does not induce a large apparent $H_1 \rightarrow \gamma\gamma$ branching ratio. The sparticle decays are obtained with `NMSDecay` [74,75] and the Higgs production cross sections at the LHC are obtained with `SusHi` `1.5.0` [76–85], interfaced with `LHAPDF` `5.9.1` [86] and using MSTW parton distribution functions (PDFs) at NNLO [87]. At the outcome of this search, phenomenologically realistic points exhibiting the characteristics which we described above are obtained and presented in Table 1.

In Table 1, we provide the input for `NMSSMTools` as well as relevant masses. The squark soft mass parameters are all chosen degenerate as $m_{\tilde{Q}}$ (for simplicity). So are also the soft masses of the sleptons, $m_{\tilde{L}}$. We observe that the Higgs mass predictions of `NMSSMTools` for very heavy sfermions may not be entirely reliable, as a resummation of large $\log(\frac{m_{\tilde{Q}}}{m_t})$ may be necessary: such effects are addressed, e.g. in [88] but the details of the correspondence between the parameters and the spectrum are of secondary importance for our conclusions. Note that all the considered points satisfy the phenomenological tests implemented within `NMSSMTools` – except maybe $(g-2)_\mu$ (satisfied for P4 and P9) – and `HiggsBounds` within 2σ. We make sure that BR$[H_1 \rightarrow A_1 A_1] < 1 \cdot 10^{-4}$. The fit values to the Higgs measurement at ~ 125 GeV obtained with `HiggsSignals` are all competitive with the SM – i.e. $\chi^2 < \chi^2_{\text{SM}}$ or $|\chi^2/\chi^2_{\text{SM}} - 1| \ll 1$.

Concerning the flavor constraints associated to $A_1 \rightarrow e^+ e^-$ or, more generally, to a mediation by A_1, we stress that the proximity in mass of A_1 to the pion would certainly require a more careful analysis on the experimental side, so that the current experimental limits are likely not to apply. Yet, for completeness, we wish to show to which extent A_1-mediated contributions to rare B and K decays can be reduced in our scenario. We thus undertook the task of tuning the parameters in the sfermion sector in order to suppress the effective flavor-changing couplings for point P2

only: it is quite clear that such a requirement can always be applied independently of the properties of the Higgs states. For this point, the trilinear Higgs-stop coupling A_t is adjusted in such a way that the effective flavor-changing A_1 couplings amount to $C_A \simeq 1.3 \cdot 10^{-6}$ GeV^2 and $C'_A \simeq 2.6 \cdot 10^{-8}$ GeV^2. These extremely suppressed numbers come at the price of the 7-digit precision in the value of A_t. We note that to simultaneously maintain $m_{H_1} \simeq 125$ GeV a significantly heavier squark sector (compared to P1) becomes necessary: this is not unexpected as it is unlikely to combine a maximal stop mixing (which provides a large contribution to m_{H_1}) and minimal effective flavor-changing A_1 couplings with the sole handle of A_t.[8] The contribution to BR$[B^0 \rightarrow K^0 e^+ e^-]$ is then at the level of $\sim 10^{-20}$ and, for BR$[K^+ \rightarrow \pi^+ e^+ e^-]$ at the level of $\sim 10^{-23}$. Such effects are far too small to be measurable experimentally. However, if we consider P1 for comparison, where the sfermion sector was not tailored to accommodate these channels, $C_A \sim 130$ GeV^2 and $C'_A \sim 3$ GeV^2, contributing to the branching ratios at the level of 10^{-4} and 10^{-7}, respectively, i.e. far beyond existing limits. Of course, the precision that we requested in the suppression of C_A and C'_A for point P2 is not really necessary in view of the $e^+ e^-$ channels: $C_A \sim 1$ GeV^2 and $C'_A \sim 0.1$ GeV^2 would be sufficient and can be achieved with the simpler requirement $A_t \simeq -8.5$ TeV for P2. Furthermore, experimental cuts would typically require $m_{e^+ e^-} > 140$ MeV [61], so that our scenario with $m_{A_1} \simeq m_{\pi^0}$ is not affected by these limits in general. However, we wish to stress that any bound on flavor transitions mediated by A_1 could be circumvented in such a fashion. Therefore, we will pay no further attention to these flavor limits on the basis that they strongly depend on the details of the sfermion sector.

We now discuss the phenomenology of the benchmark points. $\tan\beta$ ranges from 4 to 15 in Table 1: this implies a variety of regimes for the points under consideration, as we will see later. In particular, this determines the value of μ, i.e. the higgsino spectrum: the lightest neutralino mass varies between 100 GeV at $\tan\beta = 15$ (P4) to 370 GeV at $\tan\beta = 4$ (P7). κ and λ are always of order 0.1 and their ratio also depends on $\tan\beta$ (see previous section). Note that larger values of λ are accessible but tend to result in too efficient a cross section for the diphoton signal, as we shall discuss later. The values of A_κ appear with a sizable number of digits: this corresponds to the precision necessary to keep m_{A_1} within 135 ± 0.5 MeV. M_A falls within 10 to 60 GeV of 750 GeV. The squark masses are chosen, together with the trilinear coupling A_t, so as to generate a mass close to ~ 125 GeV

---

[8] The low $\tan\beta$ range is typically less sensitive to limits from flavor transitions (as $\tan\beta$ is no longer an enhancement factor). Yet, large squark masses also emerge as a necessity to generate $m_{H_1} \simeq 125$ GeV because of the lower tree-level Higgs mass $\sim M_Z \cos 2\beta$; note that tree-level NMSSM effects on the SM-like Higgs mass, using large λ or singlet–doublet mixing, are difficult to combine with our scenarios.

Table 1 Benchmark points: NMSSM input and masses; we furthermore choose the trilinear Higgs-sbottom, stau couplings as $A_{b,\tau} = 1.5$ TeV, and the gaugino mass parameters as $2M_1 = M_2 = M_3/3$

	P1	P2	P3	P4	P5	P6	P7	P8	P9
Parameters									
λ	0.1	0.08	0.08	0.06	0.15	0.21	0.2	0.13	0.05
κ	0.25	0.2	0.24	0.22	0.19	0.265	0.2	0.26	0.17
$\tan\beta$	10	10	12	15	5	5	4	8	14
μ (GeV)	150	150	127	103	296	296.5	375	188	110
M_A (GeV)	760	784	780	775	785.5	785.5	810	770	765
A_κ (GeV)	0.003059	0.0573065	0.0151443	0.0012258	0.149903	0.303953	0.4206824	0.025274	−0.0017404
$m_{\tilde{Q}}$ (TeV)	1.75	10	3	3	10	10	15	3	2
A_t (TeV)	−4	−8.519135	−5	−5	−16	−14	−35	−6	−4
$m_{\tilde{L}}$ (TeV)	0.3	0.3	0.3	0.3	0.305	0.32	0.4	0.4	0.4
M_2 (TeV)	1	1	2	1	1	1	1	1	1
Higgs spectrum									
m_{H_1} (GeV)	124	125	125	125	125	124	125	125	125
m_{H_2} (GeV)	741	740	753	748	734	726	733	738	744
m_{H_3} (GeV)	758	754	766	758	757	759	763	760	753
m_{A_1} (GeV)	0.135	0.135	0.135	0.135	0.135	0.135	0.135	0.135	0.135
m_{A_2} (GeV)	750	747	759	752	744	744	750	749	750
$m_{H^\pm}$ (GeV)	754	751	763	757	747	746	753	753	754
A_1 mixing									
P_d	0.023	0.019	0.018	0.014	0.036	0.050	0.047	0.031	0.012
Higgsinos									
$m_{\tilde{\chi}_1^0}$ (GeV)	147	149	124	100	294	294	370	185	107
$m_{\tilde{\chi}_2^0}$ (GeV)	158	160	135	111	310	311	393	197	117
$m_{\tilde{\chi}_1^\pm}$ (GeV)	152	155	130	105	303	303	384	191	112

for H_1: the values fall in the range 1–20 TeV. We have already commented the number of digits for A_t in P2: we aim to check that flavor transitions mediated by A_1 can be made arbitrarily negligible. The slepton masses are taken between 300 and 400 GeV, depending on the mass of the lightest neutralino: they matter only for $(g-2)_\mu$. Finally, we employ hierarchical gaugino masses, $2M_1 = M_2 = M_3/3 = 1$ TeV and trilinear soft couplings $A_{b,\tau} = 1.5$ TeV: they play essentially no role here.

Table 1 also provides the Higgs masses: from the discussion above, it should be clear that the parameters have been chosen so that:

- $m_{H_1} \simeq 125$ GeV corresponds to the SM-like Higgs boson, identified with the ~125 GeV signal of the LHC;
- $m_{A_1} \simeq 135$ MeV, and the A_1 should mix with π^0;
- $m_{H_2,H_3} \simeq 750$ GeV; consequently, m_{A_2} and $m_{H^\pm}$ also fall close to 750 GeV.

The only quantity deserving discussion at this level is the mass-splitting between H_2 and H_3: it ranges from ~10 to

~30 GeV, depending on the values of κ and $\tan\beta$. As we aimed at a large singlet–doublet mixing close to 50 %, this mass gap is essentially determined by Eq. (12).

Finally, we indicate the magnitude of the doublet component in A_1, P_d, which plays a central role for the characteristics of this state. It follows the approximate rule $P_d = 0.232 \cdot \lambda$, that one can infer from the tree-level definition, Eq. (2), together with the various conditions on M_A, μ, κ, and $\sin 2\beta$ presented in Sect. 2.4.

In Table 2, we indicate several Higgs branching fractions as well as the production cross sections in ggf and bbh at the LHC for the heavy states. First, we check that BR$[H_1 \rightarrow A_1 A_1] < 1 \cdot 10^{-4}$, so that no non-SM diphoton decay of H_1 conflicts with the LHC Run-I results – the total width of H_1 is always SM-like: $\Gamma_{H_1} \simeq 4 \cdot 10^{-3}$ GeV. Concerning the heavy CP-even states, their widths fall typically between 1 and 2 GeV and are dominated by the fermionic channels – $b\bar{b}$ and/or $t\bar{t}$ depending on $\tan\beta$. BR$[H_{2,3} \rightarrow A_1 A_1]$ is typically at 10–30 % and comparable for both states (due to an efficient mixing): we observe that larger values ($\gtrsim 50$ %) are accessible for larger κ (λ) but such values tend to overshoot

Table 2 Higgs branching fractions and production cross sections

	P1	P2	P3	P4	P5	P6	P7	P8	P9
Higgs decays									
$BR[H_1 \to A_1 A_1]$	$7 \cdot 10^{-6}$	$6 \cdot 10^{-5}$	$1 \cdot 10^{-5}$	$9 \cdot 10^{-6}$	$3 \cdot 10^{-6}$	$3 \cdot 10^{-7}$	$8 \cdot 10^{-6}$	$1 \cdot 10^{-6}$	$5 \cdot 10^{-6}$
Γ_{H_2} (GeV)	1.60	1.53	2.04	2.71	1.30	1.53	1.29	1.37	1.41
$BR[H_2 \to A_1 A_1]$	0.306	0.174	0.188	0.113	0.190	0.373	0.288	0.363	0.186
$BR[H_2 \to b\bar{b}]$	0.332	0.397	0.439	0.527	0.117	0.087	0.056	0.269	0.599
$BR[H_2 \to t\bar{t}]$	0.094	0.121	0.064	0.032	0.533	0.357	0.551	0.186	0.046
$BR[H_2 \to \tau\bar{\tau}]$	0.048	0.058	0.064	0.077	0.017	0.013	0.008	0.039	0.087
$BR[H_2 \to \tilde{h}\tilde{h}]$	0.012	0.004	0.003	0.003	0.021	0.040	0	0.027	0.002
Γ_{H_3} (GeV)	1.92	1.55	2.00	2.28	1.52	2.09	2.27	1.71	2.05
$BR[H_3 \to A_1 A_1]$	0.231	0.213	0.247	0.185	0.191	0.226	0.099	0.301	0.082
$BR[H_3 \to b\bar{b}]$	0.279	0.292	0.327	0.427	0.073	0.062	0.043	0.182	0.608
$BR[H_3 \to t\bar{t}]$	0.096	0.104	0.055	0.029	0.452	0.395	0.655	0.162	0.052
$BR[H_3 \to \tau\bar{\tau}]$	0.041	0.043	0.048	0.062	0.011	0.009	0.006	0.027	0.089
$BR[H_3 \to \tilde{h}\tilde{h}]$	0.165	0.154	0.135	0.090	0.112	0.123	0.002	0.222	0.087
Γ_{A_2} (GeV)	2.40	2.37	3.02	4.19	2.18	2.30	2.83	1.80	2.99
$BR[A_2 \to \tau\tau]$	0.065	0.065	0.075	0.084	0.018	0.016	0.009	0.055	0.102
Higgs production									
$\sigma^{ggf}_{8TeV}[H_2]$ (fb)	0.60	0.74	0.50	0.50	3.07	2.62	3.23	1.01	0.34
$\sigma^{bbh}_{8TeV}[H_2]$ (fb)	3.90	4.53	5.98	9.91	1.21	1.13	0.58	2.78	6.01
$\sigma^{ggf}_{8TeV}[H_3]$ (fb)	0.60	0.55	0.35	0.32	2.40	2.84	5.02	0.88	0.48
$\sigma^{bbh}_{8TeV}[H_3]$ (fb)	3.37	3.00	3.84	6.17	0.71	0.82	0.59	1.95	8.20
$\sigma^{ggf}_{13TeV}[H_2]$ (fb)	2.62	3.25	2.21	2.15	10.36	11.52	14.33	4.47	1.49
$\sigma^{bbh}_{13TeV}[H_2]$ (fb)	20.70	24.08	32.14	53.05	6.35	5.89	3.03	14.72	32.05
$\sigma^{ggf}_{13TeV}[H_3]$ (fb)	2.66	2.45	1.57	1.39	10.87	12.90	22.88	3.97	2.12
$\sigma^{bbh}_{13TeV}[H_3]$ (fb)	18.21	16.17	20.95	34.00	3.86	4.46	3.23	10.54	44.11
$\sigma^{ggf}_{13TeV}[A_2]$ (fb)	12.97	13.42	10.46	10.14	37.73	37.79	53.74	17.10	10.41
$\sigma^{bbh}_{13TeV}[A_2]$ (fb)	38.62	40.05	52.81	86.19	10.19	10.20	6.25	25.01	75.85
$\gamma\gamma$ @750 GeV									
σ^{incl}_{8TeV} (fb)	2.2	1.6	2.5	2.32	1.37	2.18	1.61	2.23	1.85
σ^{incl}_{13TeV} (fb)	11.7	8.5	13.55	12.48	5.83	10.17	7.40	11.06	9.80

the magnitude of the observed diphoton cross section. We also provide the branching ratios to higgsinos, regrouping all the decays to the lightest (next-to-lightest) neutralino and chargino states ($\tilde{h} \ni \{\tilde{\chi}^0_1, \tilde{\chi}^0_2, \tilde{\chi}^\pm_1\}$), as well as to $\tau\bar{\tau}$ – this will be discussed in Sect. 3.2 in connection with future tests of our scenario.

Regarding the production cross sections of the heavy CP-even Higgs states at the LHC, they are essentially driven by the doublet components of these states. They are shared in roughly equal proportions by the $H_{2,3}$ states, as a consequence of the ~50 % mixing. The cross section in ggf is suppressed as $\tan^{-2}\beta$ (in agreement with the $\tan^{-1}\beta$ suppression of the H_D-coupling to tops) while that in bbh varies as $\tan^2\beta$ (in accordance with the $\tan\beta$ enhancement of the H_D-coupling to bottoms): summing over both states,

the production cross section in ggf at 8 TeV follows the approximate rule $\sigma^{ggf}_{8TeV}[H_2 + H_3] \simeq (130 \text{ fb}) \tan^{-2}\beta$; that in bbh $\sigma^{bbh}_{8TeV}[H_2 + H_3] \simeq (0.07 \text{ fb}) \tan^2\beta$; at 13 TeV, $\sigma^{ggf}_{13TeV}[H_2+H_3] \simeq (600 \text{ fb}) \tan^{-2}\beta$ and $\sigma^{bbh}_{13TeV}[H_2+H_3] \simeq (0.4 \text{ fb}) \tan^2\beta$. At low $\tan\beta \sim 4$–5, the ggf channel thus dominates, while the bbh is more efficient at large $\tan\beta \sim 10$–15. Their sum is maximal at large $\tan\beta$: ~17 fb at 8 TeV and ~95 fb at 13 TeV, and it is minimal for $\tan\beta \sim 6$: ~6 fb at 8 TeV and ~30 fb at 13 TeV. The enhancement factor between 8 and 13 TeV ranges from ~4.75 at $\tan\beta = 4$ to 5.65 at $\tan\beta = 15$. Considering that the 8 TeV data did not show any significant diphoton excess at ~750 GeV, one would prefer this enhancement factor to be as large as possible, so that it avoids tensions with the limits from Run-I. An enhanced associated production with b-quarks, which

occurs at large $\tan \beta$ is thus slightly preferred since the ratio between the 13 TeV and 8 TeV production cross section is the largest for $b\bar{b}$ initial states. The production cross sections of A_2 at 13 TeV are also given. They follow coarsely the same patterns as their analogs for H_2/H_3, with a larger ggf though.

These production cross sections and branching ratios allow us to derive the relevant cross section for the $pp \to H_2(H_3) \to 2(A_1 \to \gamma\gamma)$ process (we assume BR$[A_1 \to \gamma\gamma] \simeq 0.99$): this quantity is documented for our points in the last two lines of Table 2, at 8 and 13 TeV. Depending on the characteristics of our points, $\sigma_{\text{8TeV}}^{\text{incl}} \sim 1$–2 fb and $\sigma_{\text{13TeV}}^{\text{incl}} \sim 5$–13 fb, which is the relevant order of magnitude for an interpretation of the diphoton excess. These figures shall be analyzed with further detail in the following section.

3 Collider analysis

3.1 Analysing the diphoton signal with current data

We consider resonant H_2 (H_3) production,

$$pp \to H_2(H_3) \to 2(A_1 \to \gamma\gamma) + X, \qquad (17)$$

where X stands for the rest of the event. Due to the large boost of A_1, the two photons of the A_1 decay will be very collimated and thus the opening angle between both photons in the electronic calorimeter will be well below the angular resolution of electromagnetic calorimeters [89,90]. Therefore, our final state resembles a resonant diphoton final state. The ATLAS conference note [91] studied the signature of a 125 GeV Higgs boson decaying to four photons at $\sqrt{s} = 7$ TeV with the full data set. The search estimates the efficiency of photon-pair identification as a single photon at about 85–95 % for photons with $p_T \approx 100$ GeV and mass $m_{A_1} = 100$–200 MeV. The efficiency heavily depends on the mass of the heavy resonance, as can be seen in Fig. 3, which shows the $\Delta\eta := |\eta(\gamma_1) - \eta(\gamma_2)|$ distribution of the two photons from the $A_1 \to \gamma\gamma$ decay where η denotes the pseudorapidity. The dark (blue) curve shows the result for a Higgs boson mass of 125 GeV, while the light (beige) curve for 750 GeV. As expected the opening angle of the photons from the 750 GeV resonance is much smaller compared to the 125 GeV case. However, it is difficult to determine the exact efficiency without performing a full detector simulation. Hence, we will choose $\epsilon = 90$ % in the remainder of the paper. In any case, our conclusions will not considerably change if we assume a higher efficiency as the one from the ATLAS study [91]. This means that about 80 % of all four-photon events within the fiducial region will be classified as diphoton events. This choice is further supported by the analysis in Ref. [92].
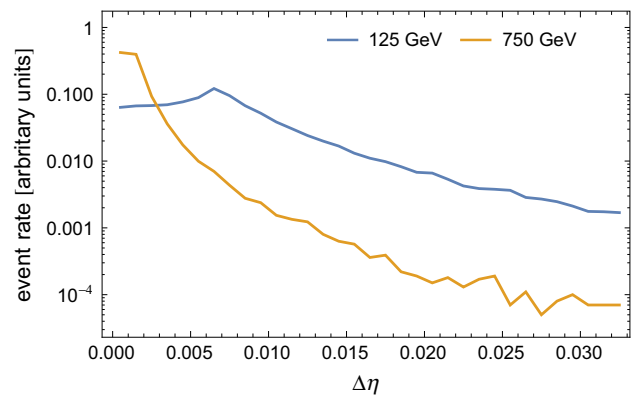
Fig. 3 The pseudorapidity separation between two photons from the A_1 decay, $m_{A_1} = 200$ MeV, for the resonance production of the SM-like Higgs boson (*dark/blue line*) and the hypothetical 750 GeV (*light/beige line*) scalar

Table 3 Selection cuts of the 13 TeV ATLAS/CMS diphoton searches [1,2]

ATLAS	CMS
$p_T(\gamma) \geq 25$ GeV	$p_T(\gamma) \geq 75$ GeV
$|\eta(\gamma)| \leq 2.37$	$|\eta(\gamma)| \leq 1.44$ or $1.57 \leq |\eta(\gamma)| \leq 2.5$ at least one γ with $|\eta(\gamma)| \leq 1.44$
$E_T^{\gamma_1}/m_{\gamma\gamma} \geq 0.4$, $E_T^{\gamma_2}/m_{\gamma\gamma} \geq 0.3$	$m_{\gamma\gamma} \geq 230$ GeV

In order to test compatibility of the parameter points with experimental results at $\sqrt{s} = 8$ TeV [93–96] and 13 TeV [1, 2] we generated parton-level events with `Madgraph 2.3.3` [97] interfaced with the Monte Carlo (MC) generator `Pythia 6.4` [98] for the parton shower and hadronization. We have implemented the 8 and 13 TeV diphoton searches from ATLAS and CMS [1,2] into the `CheckMATE 1.2.2` framework [99] with its `AnalysisManager` [100]. `CheckMATE 1.2.2` is based on the fast detector simulation `Delphes 3.10` [101] with heavily modified detector tunes and it determines the number of expected signal events passing the selection cuts of the particular analysis. The selection cuts for both ATLAS and CMS analyses are shown in Table 3. The resulting signal efficiency varies between 20 and 60 % depending on the signal region, the experiment and the center-of-mass energy.

Using the above setup we calculate the expected number of events in the signal regions centered at 750 GeV for each parameter point P1–P9 in four 8 TeV searches and in two 13 TeV searches. The results are collected in Table 4. For reference, in column two and three we provide the observed number of events above the SM background ("sig.") and the observed $S95$ exclusion limits calculated using `CheckMATE` [99,102]. Our benchmark points offer a range of cross sections for the desired signal, from 5.8 to

Table 4 Event numbers due to the heavy Higgs production in the signal regions of the ATLAS and CMS diphoton searches at $\sqrt{s} = 8$ and 13 TeV for each of the benchmark scenarios considered (we keep two separate signal regions for CMS13)

Search	Sig.	$S95$	P1	P2	P3	P4	P5	P6	P7	P8	P9
$\sqrt{s} = 13$ TeV											
ATLAS13 [1]	16.6	27	14.1	10.3	15.4	15.1	7.1	12.3	8.9	13.4	11.8
CMS13 EBEB [2]	4.5	12.8	14.4*	10.5	15.7*	15.4*	7.2	12.6	9.2	13.7*	12.1
CMS13 EBEE [2]	0	9.5	5.4	4.0	5.9	5.8	2.7	4.7	3.4	5.1	4.6
$\sqrt{s} = 8$ TeV											
ATLAS8-1407.0653 [93]	6	20	15.8	11.6	16.9	16.4	9.7	15.4	11.4	15.4	13.1
ATLAS8-1504.05511 [94]	2.6	23	21.5	15.7	22.9	22.3	13.2	20.9	15.5	20.9	17.7
CMS8-EXO-12-045 [95]	0	16	9.4	6.8	10.0	9.7	5.7	9.1	6.8	9.1	7.7
CMS8-1506.02301 [96]	3	34	16.2	11.8	17.2	16.8	9.9	15.7	11.7	15.7	13.4

For reference, we provide the observed number of signal events above the expected SM background ("sig."; 0 if the number of expected background events exceeds the number of observed events) and the observed $S95$ exclusion limits calculated using CheckMATE [100]. The event numbers marked with a * would be excluded at CL 95 % for the respective channel

12.7 fb at 13 TeV, as listed in Table 2. Points P1, P3, P4 and P8 fit exactly the claimed event rate from ATLAS [1], but predict too many events in the CMS signal region [2]; see also the discussion in [5]. The remaining points fulfill all constraints. In a model independent χ^2 fit we estimate that the best-fit cross section at 13 TeV using ATLAS and CMS results is 8.3 fb [5], with points P2 and P7 being closest in value, cf. Table 2. A similar analysis for the 8 TeV data yields 0.5 fb, while a combination of all the available data gives a range of cross sections 4.9–5.7 fb at 13 TeV. The exact result depends on the details of the production mechanism, but our benchmark points cover well the desired range. The best fit to all data is provided by point P5.

In Fig. 4, we show the diphoton invariant mass distribution of our diphoton signal for two different bin sizes. We consider benchmark point P6 for illustration. The distribution with the large bin size of 40 GeV corresponds to the experimental bin size of the ATLAS study [1], as shown in the left panel. The experimental photon energy resolution of about 5–10 % would allow for a higher precision [103] but due to the small statistical sample, both experiments have to choose a rather large bin size. One can clearly see that our benchmark point with two scalars cannot be distinguished from a wide resonance with the current data. For comparison we have included into this plot the original data from ATLAS after subtracting the expected background. One can see that the events predicted for our P6 benchmark provide a good reproduction of the experimental shape. We also display in the right panel of Fig. 4 the invariant mass distribution with a 5 GeV binning. While currently the experimental resolution in $m_{\gamma\gamma}$ exceeds 10 GeV, one can speculate that further improvements during the current LHC run will be made. With the accuracy of ∼5 GeV and an increased luminosity, the broad excess, provided it is real, might be resolved as two narrow resonances [8].

Our estimate of the number of signal events in Table 4 has a theoretical uncertainty. The choice of the parton distribution function, missing higher-order calculations and the details of the parton shower as well as the fragmentation induce an uncertainty on the signal rate. However, our final-state configuration is relatively simple and thus the details of the MC tuning will not significantly alter our results. The size of the uncertainty from the PDFs can be sizable. The variation between the different PDFs changes the hadronic cross section. In addition, the scale dependence of the production cross section on the renormalization and factorization scale affects the signal rate. We estimate the sum of these effects to be of the order of 10 % [104]. Furthermore, the normalization can heavily depend on the value of the bottom Yukawa coupling [104]. Finally, we did not model the detector response of identifying a photon from the pseudoscalar decay into the diphoton state but rather choose a flat efficiency factor of $\epsilon = 90$ %. Here, one can assume a conservative uncertainty of about 20 % on the signal rate due to the uncertainty in the photon identification. We conclude that the total uncertainty is of the order of $\mathcal{O}(20)$ %, plus an additional uncertainty from the definition of the bottom quark mass.

3.2 Future directions

So far we have assumed that our signal in Eq. (17) mimics the diphoton signal since the two collimated photons of the light-pseudoscalar decay are indistinguishable from an isolated photon. However, if the four-photon final state was discriminated from the diphoton signature, it would be a strong hint at our scenario. References [105–107] considered photon jets (two or more collimated photons) at hadron colliders. In particular, Ref. [107] discussed the possibility of photon conversion into e^+e^- pairs and its discriminating power between photon jets and isolated photons. For a photon jet, the prob-
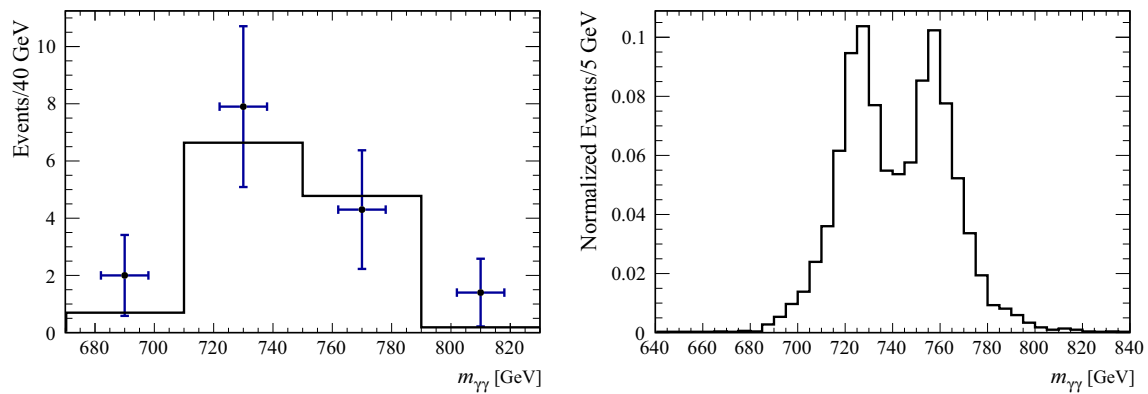
Fig. 4 Invariant mass distribution of the diphoton resonance of benchmark point P6 (*black histograms*). *Left* a bin size of 40 GeV corresponding to the experimental bin size of the ATLAS search [1] and the number of events over background with errors obtained by ATLAS for each point (*blue*). *Right* a bin size of 5 GeV showing a twin-peak feature

ability of photon conversion is higher than for a single photon, and Ref. [107] showed that already several tens of events are sufficient to discriminate between both hypotheses and a few hundred events allow for a 5σ discrimination assuming prompt photons. However, their conclusions assume a pseudoscalar mass of 1 GeV and the results are very sensitive to this parameter. For long-lived pseudoscalars, the discriminating power is reduced since photon conversion cannot start before the pseudoscalar decay. As a consequence, the discriminating power becomes worse for increasing lifetimes.

Apart from the diphoton signal, which is the main motivation of the current study, the NMSSM parameter points discussed here also have additional distinctive features closely related to the diphoton signal. We shortly discuss these collider signatures.

As discussed in the previous section, the light pseudoscalar, A_1, has a small branching fraction of $\lesssim 1$ % for decays to electron pairs. Because of its short life-time it would typically decay promptly to a highly collimated e^+e^- pair, so-called "electron jet". Such electron jets, prompt or displaced, were searched for by the LHC experiments as they can appear in many different models of new physics. In our case, two signatures can appear: two high-p_T electron jets or one electron jet and an energetic photon. Note that even though we have suppressed the branching ratio of the SM-like Higgs boson to pseudoscalars such a signal is also possible apart from the decays of the heavy Higgs states. For the 125 GeV Higgs an associated production of $pp \rightarrow hW(\rightarrow \ell\nu)$ (where h denotes the SM-like Higgs boson) was studied by ATLAS [108]. The obtained limit is weak and together with the already mentioned suppression of $H_1 \rightarrow A_1 A_1$ this is an unlikely discovery channel. The searches for the direct production of the scalar decaying to two electron jets could provide further constraints, but the limits have been obtained only for the light SM-like

Higgs boson [109,110]. Nevertheless this signature might become interesting in the current run once the diphoton signal is firmly confirmed. Corresponding studies directly applicable to the heavy Higgs particles have also been performed [111,112]. It is interesting to note that for a hypothetical scenario with a 1 TeV scalar resonance, the sensitivity of the CMS search [111] is in the fb range. While the discussed 8 TeV searches lack the sensitivity to constrain our scenario now, they clearly offer interesting prospects for observing electron decay modes of A_1 (possibly accompanied by the photon jet from the opposite decay chain) at the increased center-of-mass energy and the high luminosity run of the LHC.

Our scenario can also be probed via the "classic signature" for additional heavy neutral Higgs bosons, $pp \rightarrow \Phi \rightarrow \tau^+\tau^-$, where the limits are set in the m_Φ–$\tan\beta$ space. Within the MSSM, assuming the additional Higgs bosons at a mass around $\sim$750 GeV, the (expected) limits on $\tan\beta$ are around $\sim$35 based on Run I data [113–115] (see also [116]). In our NMSSM scenario we have three Higgs bosons with a mass around 750 GeV contributing to this search channel, H_2, H_3, and A_2, where the overall number of $\tau^+\tau^-$ events is roughly 25 % lower than in the MSSM, mainly due to the decay of $H_{2,3} \rightarrow A_1 A_1$. Consequently, a similar, but slightly higher limit on $\tan\beta$ can be set in our NMSSM scenario. With increasing luminosity this limit could roughly improve to $\tan\beta \sim$ 5–10 at the LHC after collecting 300–3000/fb of integrated luminosity (see also [117]). Therefore, the proposed scenario could eventually lead to an observable signal in the $\tau^+\tau^-$ searches for heavy Higgs bosons at the LHC, depending on the details of the scenario (value of $\tan\beta$, masses of electroweak particles etc.).

Another prediction that arises for parameter points considered in this study are light higgsinos. With the masses of 100–300 GeV they are well within the kinematic reach of

the LHC. However, the small mass differences, $\mathcal{O}(10\,\text{GeV})$, within the light higgsino sector hinder their observation at the LHC. If all the non-higgsino SUSY particles are sufficiently far in mass (points P1–P4, P8, P9), the decay of the second neutralino, $\tilde{\chi}_2^0$ proceeds almost exclusively via the light pseudoscalar A_1. With the following significant branching ratio to a soft $\gamma\gamma$ pair the observation in the soft di- and trilepton searches [118,119] becomes practically impossible. The radiative production at a high-energy e^+e^- collider remains a valid possibility though [120,121].

Finally, light smuons are required in order to obtain phenomenologically viable muon anomalous magnetic moment and to counteract the effects of a very light pseudoscalar. For our parameter points we fix slepton masses at 300–400 GeV. While this is close to the existing simplified model limits, see e.g. [122], in our case due to the significant branching ratio $\text{BR}(\tilde{\ell}_L \to \tilde{\chi}_1^\pm \nu) \gtrsim 50\,\%$ these constraints are significantly relaxed. Nevertheless, if the slepton and higgsino spectra are favorable, the observation in the current LHC run is plausible.

4 Conclusions

We have proposed an NMSSM scenario that can explain the excess in the diphoton spectrum at 750 GeV recently observed by ATLAS and CMS. In our scenario the heavy neutral (and charged) Higgs bosons have a mass around $\sim$750 GeV, while one light CP-odd Higgs boson has a mass around the mass of the pion, $\sim$135 MeV. The 750 GeV excess is generated by the production of the heavy neutral CP-even Higgs bosons, which subsequently decay to two light pseudoscalars. Each of these pseudoscalars then decays, mainly via the mixing with the π^0, to a collimated photon pair that appears as a single photon in the electromagnetic calorimeter. The mass gap between heavy Higgses of $\mathcal{O}(20)$ GeV mimics a large width of the 750 GeV peak. Furthermore, the production of the heavy neutral CP-even Higgs bosons may contain a large component of $b\bar{b}$ initial state, thus ameliorating a possible tension with 8 TeV data compared to other production modes. The main virtue of our scenario is that all necessary properties to fit the signal can be united in a phenomenologically realistic way within as theoretically simple a model as the NMSSM, without e.g. requiring additional ad hoc matter.

We derived the NMSSM parameter space in which this scenario can be realized. It is characterized by a heavy Higgs boson mass scale, M_A, around 750 GeV. The Yukawa-like couplings λ and κ are found to satisfy $\frac{0.4\tan\beta}{1+\tan^2\beta} \lesssim \lambda \lesssim \frac{2\sqrt{2}\tan\beta}{\sqrt{1+18\tan^2\beta+\tan^4\beta}}$ and $\kappa \simeq \frac{\lambda}{2\sin 2\beta}$. The μ parameter is given by $\mu \sim M_A \sin 2\beta$, or $2\frac{\kappa}{\lambda}\mu \simeq 750$ GeV. We furthermore find $5 \lesssim \tan\beta \lesssim 15$, $A_\kappa \lesssim \mathcal{O}(0.1)$ GeV, and $A_\lambda \ll v$. Due to this choice of parameters the two neutral heavy CP-even Higgs bosons are strongly mixed doublet/singlet states

and the light CP-odd Higgs boson can have a mass around m_π. The light CP-even Higgs boson with SM-like properties can have a mass around $\sim$125 GeV, mainly by choosing the scalar top parameters accordingly. The parameter choice furthermore forbids a large decay rate of the SM-like Higgs boson to the two light CP-odd states, which would be in contradiction with the LHC measurements.

In order to validate our scenario we have chosen nine benchmark points, all satisfying the above constraints, but with a strong variation within the allowed intervals. Using state-of-the-art tools, including higher-order corrections, these points have been analyzed to reproduce the observed "excess" in the diphoton search at the LHC Run-II, including detector simulation and efficiencies. We have furthermore checked explicitly that these points fulfill all other experimental constraints. These include LHC Higgs (and SUSY) searches, Higgs boson rate measurements, as well as flavor observables and electroweak precision data. We have shown explicitly that the two collimated photon pairs would be seen as a single photon each, applying the same settings as in the ATLAS/CMS analyses.

Finally, we have analyzed how our scenario can be probed in the upcoming continued LHC Run-II. Possibly striking features are the absence of any other relevant decay mode, such as the decay to massive gauge bosons, as well as an increased rate of photon conversion to electron jets with respect to the "simple" diphoton decay mode, or the distinction of a photon pair from a single photon. Furthermore, the heavy neutral Higgs bosons should be visible in the conventional $\tau^+\tau^-$ searches at high luminosity. Other characteristic features of our scenario are relatively light higgsinos and possibly sleptons that can be probed at the LHC Run-II. Using these characteristics, our scenario should be distinguishable from most other physics scenarios that have been proposed to explain the LHC diphoton "excess".

References

1. The ATLAS Collaboration, ATLAS-CONF-2015-081
2. The CMS Collaboration, CMS PAS EXO-15-004
3. L.D. Landau, Dokl. Akad. Nauk Ser. Fiz. **60**(2), 207 (1948)
4. C.-N. Yang, Phys. Rev. **77**, 242 (1950)
5. J.S. Kim, K. Rolbiecki, R.R. de Austri. EPJC (2016, to appear). arXiv:1512.06797 [hep-ph]
6. J.S. Kim, J. Reuter, K. Rolbiecki, R.R. de Austri. Phys. Lett. B **755**, 403–408 (2016). arXiv:1512.06083 [hep-ph]
7. V. De Romeri, J.S. Kim, V. Martin-Lozano, K. Rolbiecki, R.R. de Austri. (2016). arXiv:1603.04479 [hep-ph]
8. Q.H. Cao, Y.Q. Gong, X. Wang, B. Yan, L.L. Yang. (2016). arXiv:1601.06374 [hep-ph]
9. A. Angelescu, A. Djouadi, G. Moreau. Phys. Lett. B **756**, 126–132 (2016). arXiv:1512.04921 [hep-ph]
10. A. Falkowski, O. Slone, T. Volansky. JHEP **1602**, 152 (2016). arXiv:1512.05777 [hep-ph]
11. F. Staub et al. (2016). arXiv:1602.05581 [hep-ph]
12. M. Drees, R. Godbole, P. Roy, *Hackensack* (World Scientific, USA, 2004), p. 555
13. R.S. Gupta, S. Jaeger, Y. Kats, G. Perez, E. Stamou. (2015). arXiv:1512.05332 [hep-ph]
14. S.F. King, R. Nevzorov. JHEP **1603**, 139 (2016). arXiv:1601.07242 [hep-ph]
15. Y.L. Tang, S.H. Zhu. (2015). arXiv:1512.08323 [hep-ph]
16. L.J. Hall, K. Harigaya, Y. Nomura. JHEP **1603**, 017 (2016). arXiv:1512.07904 [hep-ph]
17. E. Ma. (2015). arXiv:1512.09159 [hep-ph]
18. F. Wang, W. Wang, L. Wu, J. M. Yang, M. Zhang. (2015). arXiv:1512.08434 [hep-ph]
19. B.C. Allanach, P.S.B. Dev, S.A. Renner, K. Sakurai. (2015). arXiv:1512.07645 [hep-ph]
20. R. Ding, L. Huang, T. Li, B. Zhu. (2015). arXiv:1512.06560 [hep-ph]
21. B. Bellazzini, R. Franceschini, F. Sala, J. Serra. JHEP **1604**, 072 (2016). arXiv:1512.05330 [hep-ph]
22. C. Petersson, R. Torre. Phys. Rev. Lett. **116**(15), 151804 (2016). arXiv:1512.05333 [hep-ph]
23. J.A. Casas, J.R. Espinosa, J.M. Moreno. (2015). arXiv:1512.07895 [hep-ph]
24. U. Ellwanger, C. Hugonie, A.M. Teixeira, Phys. Rept. **496**, 1 (2010). arXiv:0910.1785 [hep-ph]
25. M. Maniatis, Int. J. Mod. Phys. A **25**, 3505 (2010). arXiv:0906.0777 [hep-ph]
26. J.E. Kim, H.P. Nilles, Phys. Lett. B **138**, 150 (1984)
27. G. Aad et al. [ATLAS Collaboration], Phys. Lett. B **716**, 1 (2012). arXiv:1207.7214 [hep-ex]
28. S. Chatrchyan et al. [CMS Collaboration], Phys. Lett. B **716**, 30 (2012). arXiv:1207.7235 [hep-ex]
29. F. Domingo, G. Weiglein. JHEP **1604**, 095 (2016). arXiv:1509.07283 [hep-ph]
30. X.J. Bi et al. (2015). arXiv:1512.08497 [hep-ph]
31. S. Knapen, T. Melia, M. Papucci, K. Zurek. Phys. Rev. D **93**(7), 075020 (2016). arXiv:1512.04928 [hep-ph]
32. P. Agrawal, J. Fan, B. Heidenreich, M. Reece, M. Strassler. (2015). arXiv:1512.05775 [hep-ph]
33. B.A. Dobrescu, G.L. Landsberg, K.T. Matchev, Phys. Rev. D **63**, 075003 (2001). arXiv:hep-ph/0005308
34. F. Larios, G. Tavares-Velasco, C.P. Yuan, Phys. Rev. D **66**, 075006 (2002). arXiv:hep-ph/0205204
35. S. Chang, P.J. Fox, N. Weiner, Phys. Rev. Lett. **98**, 111802 (2007). arXiv:hep-ph/0608310
36. J. Chang, K. Cheung, C.T. Lu. Phys. Rev. D **93**(7), 075013 (2016). arXiv:1512.06671 [hep-ph]
37. U. Ellwanger, C. Hugonie. (2016). arXiv:1602.03344 [hep-ph]
38. The ATLAS Collaboration, ATLAS-CONF-2013-090, ATLAS-COM-CONF-2013-107
39. The CMS Collaboration, CMS-PAS-HIG-14-020
40. R. Barate et al. [LEP Working Group for Higgs boson searches and ALEPH and DELPHI and L3 and OPAL Collaborations], Phys. Lett. B **565**, 61 (2003). arXiv:hep-ex/0306033
41. LEP Higgs working group, Eur. Phys. J. C **47**, 547 (2006). arXiv:hep-ex/0602042
42. M. Gell-Mann, R.J. Oakes, B. Renner, Phys. Rev. **175**, 2195 (1968)
43. Q. Chang, Y.D. Yang, Phys. Lett. B **676**, 88 (2009). arXiv:0808.2933 [hep-ph]
44. P. Masjuan, P. Sanchez-Puertas. arXiv:1512.09292 [hep-ph]
45. A.M. Bernstein, B.R. Holstein, Rev. Mod. Phys. **85**, 49 (2013). arXiv:1112.4809 [hep-ph]
46. H.W. Atherton et al., Phys. Lett. B **158**, 81 (1985)
47. K.A. Olive et al. [Particle Data Group Collaboration], Chin. Phys. C **38**, 090001 (2014)
48. E. Abouzaid et al. [KTeV Collaboration], Phys. Rev. D **75**, 012004 (2007). arXiv:hep-ex/0610072
49. A.E. Dorokhov, M.A. Ivanov, Phys. Rev. D **75**, 114007 (2007). arXiv:0704.3498 [hep-ph]
50. Y. Kahn, M. Schmitt, T.M.P. Tait, Phys. Rev. D **78**, 115002 (2008). arXiv:0712.0007 [hep-ph]
51. The ATLAS and CMS Collaborations, ATLAS-CONF-2015-044
52. U. Ellwanger, Talk given at KUTS 4 (Heidelberg, Germany), 21.01.2016. https://sites.google.com/site/kutsmh/home/heidelberg
53. H. Baer, R. Dermisek, S. Rajagopalan, H. Summy, JCAP **1007**, 014 (2010). arXiv:1004.3297 [hep-ph]
54. S. Profumo, P. Ullio, JCAP **0311**, 006 (2003). arXiv:hep-ph/0309220
55. M. Fujii, K. Hamaguchi, Phys. Lett. B **525**, 143 (2002). arXiv:hep-ph/0110072
56. LEPSUSYWG, ALEPH, DELPHI, L3 and OPAL experiments, note LEPSUSYWG/01-03.1. http://lepsusy.web.cern.ch/lepsusy/Welcome.html
57. F. Wilczek, Phys. Rev. Lett. **40**, 279 (1978)
58. J. Jaeckel, M. Spannowsky, Phys. Lett. B **753**, 482 (2016). arXiv:1509.00476 [hep-ph]
59. S. Andreas, O. Lebedev, S. Ramos-Sanchez, A. Ringwald, JHEP **1008**, 003 (2010). arXiv:1005.3978 [hep-ph]
60. G. Hiller, Phys. Rev. D **70**, 034018 (2004). arXiv:hep-ph/0404220
61. J.R. Batley et al. [NA48/2 Collaboration], Phys. Lett. B **677**, 246 (2009). arXiv:0903.3130 [hep-ex]
62. F. Domingo. (2015). arXiv:1512.02091 [hep-ph]
63. F. Bergsma et al. [CHARM Collaboration], Phys. Lett. B **157**, 458 (1985)
64. F. Domingo, U. Ellwanger, JHEP **0807**, 079 (2008). arXiv:0806.0733 [hep-ph]
65. U. Ellwanger, J.F. Gunion, C. Hugonie, JHEP **0502**, 066 (2005). arXiv:hep-ph/0406215
66. U. Ellwanger, C. Hugonie, Comput. Phys. Commun. **175**, 290 (2006). arXiv:hep-ph/0508022
67. U. Ellwanger, C. Hugonie, Comput. Phys. Commun. **175**, 290 (2006). arXiv:hep-ph/0508022. http://www.th.u-psud.fr/NMHDECAY/nmssmtools.html
68. G. Degrassi, P. Slavich, Nucl. Phys. B **825**, 119 (2010). arXiv:0907.4682 [hep-ph]
69. P. Bechtle, O. Brein, S. Heinemeyer, G. Weiglein, K.E. Williams, Comput. Phys. Commun. **181**, 138 (2010). arXiv:0811.4169 [hep-ph]
70. P. Bechtle, O. Brein, S. Heinemeyer, G. Weiglein, K.E. Williams, Comput. Phys. Commun. **182**, 2605 (2011). arXiv:1102.1898 [hep-ph]

71. P. Bechtle, O. Brein, S. Heinemeyer, O. Stål, T. Stefaniak, G. Weiglein, K. Williams, PoS CHARGED **2012**, 024 (2012). arXiv:1301.2345 [hep-ph]

72. P. Bechtle, O. Brein, S. Heinemeyer, O. Stål, T. Stefaniak, G. Weiglein, K.E. Williams, Eur. Phys. J. C **74**, 2693 (2014). arXiv:1311.0055 [hep-ph]. http://higgsbounds.hepforge.org/

73. P. Bechtle, S. Heinemeyer, O. Stål, T. Stefaniak, G. Weiglein, Eur. Phys. J. C **74**, 2711 (2014). arXiv:1305.1933 [hep-ph]

74. M. Muhlleitner, A. Djouadi, Y. Mambrini, Comput. Phys. Commun. **168**, 46 (2005). arXiv:hep-ph/0311167

75. D. Das, U. Ellwanger, A.M. Teixeira, Comput. Phys. Commun. **183**, 774 (2012). arXiv:1106.5633 [hep-ph]

76. S. Liebler, Eur. Phys. J. C **75**(5), 210 (2015). arXiv:1502.07972 [hep-ph]

77. R.V. Harlander, S. Liebler, H. Mantler, Comput. Phys. Commun. **184**, 1605 (2013). arXiv:1212.3249 [hep-ph]

78. R. Harlander, P. Kant, JHEP **0512**, 015 (2005). arXiv:hep-ph/0509189

79. R.V. Harlander, W.B. Kilgore, Phys. Rev. D **68**, 013001 (2003). arXiv:hep-ph/0304035

80. R.V. Harlander, W.B. Kilgore, Phys. Rev. Lett. **88**, 201801 (2002). arXiv:hep-ph/0201206

81. U. Aglietti, R. Bonciani, G. Degrassi, A. Vicini, Phys. Lett. B **595**, 432 (2004). arXiv:hep-ph/0404071

82. R. Bonciani, G. Degrassi, A. Vicini, Comput. Phys. Commun. **182**, 1253 (2011). arXiv:1007.1891 [hep-ph]

83. G. Degrassi, P. Slavich, JHEP **1011**, 044 (2010). arXiv:1007.3465 [hep-ph]

84. G. Degrassi, S. Di Vita, P. Slavich, JHEP **1108**, 128 (2011). arXiv:1107.0914 [hep-ph]

85. G. Degrassi, S. Di Vita and P. Slavich, Eur. Phys. J. C **72**, 2032 (2012). arXiv:1204.1016 [hep-ph]. http://sushi.hepforge.org/

86. M.R. Whalley, D. Bourilkov, R. C. Group. arXiv:hep-ph/0508110. https://lhapdf.hepforge.org/

87. A.D. Martin, W.J. Stirling, R.S. Thorne, G. Watt, Eur. Phys. J. C **63**, 189 (2009). arXiv:0901.0002 [hep-ph]

88. P. Drechsel, L. Galeta, S. Heinemeyer, G. Weiglein. PoS EPS-HEP **2015**, 186 (2015). arXiv:1601.08100 [hep-ph]

89. G. Aad et al. [ATLAS Collaboration], Phys. Rev. D **83**, 052005 (2011). arXiv:1012.4389 [hep-ex]

90. V. Khachatryan et al. [CMS Collaboration], JINST **10**(08), P08010 (2015). arXiv:1502.02702 [physics.ins-det]

91. The ATLAS Collaboration, ATLAS-CONF-2012-079

92. L. Aparicio, A. Azatov, E. Hardy, A. Romanino, (2016). arXiv:1602.00949 [hep-ph]

93. G. Aad et al. [ATLAS Collaboration], Phys. Rev. Lett. **113**(17), 171801 (2014). arXiv:1407.6583 [hep-ex]

94. G. Aad et al. [ATLAS Collaboration], Phys. Rev. D **92**(3), 032004 (2015). arXiv:1504.05511 [hep-ex]

95. The CMS Collaboration, CMS-PAS-EXO-12-045

96. V. Khachatryan et al. [CMS Collaboration], Phys. Lett. B **750**, 494 (2015). arXiv:1506.02301 [hep-ex]

97. J. Alwall et al., JHEP **1407**, 079 (2014). arXiv:1405.0301 [hep-ph]

98. T. Sjostrand, S. Mrenna, P.Z. Skands, JHEP **0605**, 026 (2006). arXiv:hep-ph/0603175

99. M. Drees, H. Dreiner, D. Schmeier, J. Tattersall, J.S. Kim, Comput. Phys. Commun. **187**, 227 (2014). arXiv:1312.2591 [hep-ph]

100. J.S. Kim, D. Schmeier, J. Tattersall, K. Rolbiecki, Comput. Phys. Commun. **196**, 535 (2015). arXiv:1503.01123 [hep-ph]

101. J. de Favereau et al. [DELPHES 3 Collaboration], JHEP **1402**, 057 (2014). arXiv:1307.6346 [hep-ex]

102. A.L. Read, J. Phys. G **28**, 2693 (2002)

103. G. Aad et al. [ATLAS Collaboration], Eur. Phys. J. C **74**(10), 3071 (2014). arXiv:1407.5063 [hep-ex]

104. S. Heinemeyer et al. [LHC Higgs Cross Section Working Group Collaboration]. (2013). arXiv:1307.1347 [hep-ph]

105. S.D. Ellis, T.S. Roy, J. Scholtz, Phys. Rev. D **87**(1), 014015 (2013). arXiv:1210.3657 [hep-ph]

106. S.D. Ellis, T.S. Roy, J. Scholtz, Phys. Rev. Lett. **110**(12), 122003 (2013). arXiv:1210.1855 [hep-ph]

107. B. Dasgupta, J. Kopp, P. Schwaller. (2016). arXiv:1602.04692 [hep-ph]

108. G. Aad et al. [ATLAS Collaboration], New J. Phys. **15**, 043009 (2013). arXiv:1302.4403 [hep-ex]

109. G. Aad et al. [ATLAS Collaboration], JHEP **1411**, 088 (2014). arXiv:1409.0746 [hep-ex]

110. G. Aad et al. [ATLAS Collaboration]. JHEP **1602**, 062 (2016). arXiv:1511.05542 [hep-ex]

111. V. Khachatryan et al. [CMS Collaboration], Phys. Rev. D **91**(5), 052012 (2015). arXiv:1411.6977 [hep-ex]

112. G. Aad et al. [ATLAS Collaboration], Phys. Rev. D **92**(7), 072004 (2015). arXiv:1504.05162 [hep-ex]

113. V. Khachatryan et al. [CMS Collaboration], JHEP **1410**, 160 (2014). arXiv:1408.3316 [hep-ex]

114. The CMS Collaboration, CMS-PAS-HIG-14-029

115. G. Aad et al. [ATLAS Collaboration], JHEP **1411**, 056 (2014). arXiv:1409.6064 [hep-ex]

116. P. Bechtle, S. Heinemeyer, O. Stål, T. Stefaniak, G. Weiglein, Eur. Phys. J. C **75**(9), 421 (2015). arXiv:1507.06706 [hep-ph]

117. A. Holzner [ATLAS and CMS Collaborations], arXiv:1411.0322 [hep-ex]

118. V. Khachatryan et al. [CMS Collaboration], arXiv:1512.08002 [hep-ex]

119. M. van Beekveld, W. Beenakker, S. Caron, R.R. de Austri. (2016). arXiv:1602.00590 [hep-ph]

120. M. Berggren, F. Brümmer, J. List, G. Moortgat-Pick, T. Robens, K. Rolbiecki, H. Sert, Eur. Phys. J. C **73**(12), 2660 (2013). arXiv:1307.3566 [hep-ph]

121. G. Moortgat-Pick et al., Eur. Phys. J. C **75**(8), 371 (2015). arXiv:1504.01726 [hep-ph]

122. G. Aad et al. [ATLAS Collaboration], JHEP **1405**, 071 (2014). arXiv:1403.5294 [hep-ex]